J. Fluid Mech. (1996), *vol.* 313, *pp.* 309–341

Simple shear flows of dense gas–solid suspensions at finite Stokes numbers

By ASHOK S. SANGANI[1], GUOBIAO MO[1], HENG-KWONG TSAO[2] AND DONALD L. KOCH[2]

[1]Department of Chemical Engineering and Materials Science, Syracuse University, Syracuse, NY 13244, USA

[2]School of Chemical Engineering, Cornell University, Ithaca, NY 14853, USA

(Received 7 April 1995 and in revised form 9 November 1995)

We examine the problem of determining the particle-phase velocity variance and rheology of sheared gas–solid suspensions at small Reynolds numbers and finite Stokes numbers. Our numerical simulations take into account the Stokes flow interactions among particles except for pairs of particles with a minimum gap width comparable to or smaller than the mean free path of the gas molecules for which the usual lubrication approximation breaks down and particle collisions occur in a finite time. The simulation results are compared to the predictions of two theories. The first is an asymptotic theory for large Stokes number St and nearly elastic collisions, i.e. $St \gg 1$ and $0 \leqslant 1 - e \ll 1$, e being the coefficient of restitution. In this limit, the particle velocity distribution is close to an isotropic Maxwellian and the velocity variance is determined by equating the energy input in shearing the suspension to the energy dissipation by inelastic collisions and viscous effects. The latter are estimated by solving the Stokes equations of motion in suspensions with the hard-sphere equilibrium spatial and velocity distribution while the shear energy input and energy dissipation by inelastic effects are estimated using the standard granular flow theory (i.e. $St = \infty$). The second is an approximate theory based on Grad's moments method for which St and $1 - e$ are $O(1)$. The two theories agree well with each other at higher values of volume fraction ϕ of particles over a surprisingly large range of values of St. For smaller ϕ, however, the two theories deviate significantly except at sufficiently large St. A detailed comparison shows that the predictions of the approximate theory based on Grad's method are in excellent agreement with the results of numerical simulations.

1. Introduction

We examine shear flow of a suspension of spherical particles in a viscous gas under conditions of vanishingly small Reynolds number Re and finite Stokes number St. Here, $Re = \rho\gamma a^2/\mu$ and $St = \gamma\tau_v$ where ρ and μ are, respectively, the density and viscosity of the gas, γ is the magnitude of the shear rate, $\tau_v = m/(6\pi\mu a)$ is the viscous relaxation time of the particle velocity, a is the radius, and m is the mass of the particles.

Tsao & Koch (1995) recently examined this situation for the special case of dilute suspensions for which the volume fraction ϕ of the particles is small compared to unity. These investigators assumed that the hydrodynamic interactions among particles in

a dilute suspension would be negligible so that the motion of an individual particle could be modelled using Stokes drag law for an isolated particle. The only particle interactions considered were elastic collisions. These approximations can be justified at sufficiently large St and small ϕ. It was shown that dilute gas–solid suspensions show a surprisingly complex behaviour even under these simplifying assumptions. For example, two very different steady states occur depending upon St, ϕ, and the initial velocity distribution of the particles: an ignited state, in which the variance of the particle velocity is very large; and a quenched state, in which most of the particles move with the local gas velocity. The ignited state is observed only for $St > \sqrt{24}$, while multiple steady states for fixed St and ϕ exist for very dilute suspensions with $\phi < 1.5St^{-3}$ and $St > \sqrt{24}$. On the other hand, only the quenched state exists for $St < \sqrt{24}$. These investigators developed a kinetic theory to explain these and other interesting observations obtained from simple numerical simulations which neglected the hydrodynamic interactions among particles.

The present investigation has three objectives. First, to show that the theory of Tsao & Koch (1995) applies even when the hydrodynamic interactions among particles are taken into account at finite St; second, to extend the theory to higher particle volume fractions; and third, to account for the case in which the collisions between particles are not perfectly elastic but characterized instead by a conventional coefficient of restitution e. The purpose of the last objective is to supplement the theory of rapidly sheared granular flows ($St = \infty$, $e \neq 1$) by including the effects of viscous dissipation. Since the theory of granular flows has been developed to a great extent through a series of excellent papers in recent years (e.g. Jenkins & Savage 1983; Lun *et al.* 1984; Jenkins & Richman 1985; Walton & Braun 1986; Campbell 1989), our primary emphasis will on the effects of finite St.

The hydrodynamic interactions are determined by solving the Stokes equations of motion using the method described in Mo & Sangani (1994) and Sangani & Mo (1994). However, when a pair of particles approach each other within a distance comparable to the mean free path λ of the gas molecules, the Stokes equations no longer adequately describe the interactions, and, to account for this, we adopt a model in which the viscous forces on the particles with a minimum spacing less than $2\epsilon_m a$ are assumed to be the same as those acting on particles having a spacing $2\epsilon_m a$. Thus, the simulations are carried out with three parameters: St, ϕ and ϵ_m. The last of these parameters can be related to λ/a using results of calculations of the non-continuum lubrication problem (Sundararajakumar & Koch 1996).

The simulations are compared to two theories. The first is an asymptotic theory for large Stokes numbers and small inelasticity, i.e. $St \gg 1$ and $1 - e \ll 1$. In this limit, the particle velocity distribution is an isotropic Maxwellian to leading order with a particle-phase temperature T, defined as one-third the particle velocity variance. The energy input in shearing the suspension is readily expressed in terms of T through a standard expression for the viscosity of a dense gas while the viscous energy dissipated is expressed in terms of T and a non-dimensional dissipation coefficient R_{diss}, which as a function of ϕ and λ/a (or equivalently ϵ_m) is determined from an ensemble average for a suspension with a hard-sphere distribution of spatial position and an isotropic Maxwellian velocity distribution. This theory is applicable to any linear shear flow. The second is an approximate theory for simple shear flow with finite $1 - e$, St, and ϕ. This theory is based on a moment method introduced by Grad (1949) according to which the particle velocity distribution is assumed to be given by a truncated Hermite polynomial with unknown second moments of the distribution. These moments are then determined from conservation equations for the second moments of the particle

fluctuation velocities. This theory agrees well with the theory of Tsao & Koch when ϕ is small and with the aforementioned asymptotic theory when St is large and ϕ is $O(1)$. The two theories are in very good agreement with each other at higher volume fractions of particles over a surprisingly large range of values of St. For smaller ϕ, however, the theories deviate significantly from each other. The predictions based on Grad's method are found to be in excellent agreement with the results of numerical simulations over a wide range of values of ϕ, St/R_{diss}, and e. This is remarkable in view of the fact that the theory presented here represents a relatively minor modification to the existing granular flow theory while the Stokesian interactions among particles are generally far more complicated in nature compared with the solid-body collisional interactions in granular flow. The success of the approximate theory suggests that the most important role of hydrodynamic interactions is simply to set the rate of energy dissipation.

The organization of the paper is as follows. In §2, we give a brief statement of the problem and the governing equations. In §3, we present the asymptotic theory for St large compared to unity and e close to unity, and the numerical results for R_{diss} as a function of ϕ and λ/a. In §4, we present an approximate theory for arbitrary St and ϕ based on Grad's moment method. In §5, we compare the theories with the results of numerical simulations. Finally, in §6 we consider the case of finite St and $1-e$.

2. Governing equations

As mentioned in the Introduction, we consider the motion of gas-solid suspensions under imposed shear in the absence of gravity. The velocity v_i of the gas satisfies the Stokes equations of motion

$$\mu\nabla^2 v_i = \frac{\partial p}{\partial x_i}, \qquad \frac{\partial v_i}{\partial x_i} = 0, \tag{2.1}$$

where p is the pressure at point x_i and μ is the viscosity of the gas. The ensemble-averaged velocity of the particles is given by

$$\langle U_i \rangle = \gamma_{ij} x_j, \tag{2.2}$$

where γ_{ij} is the mean velocity gradient. The motion of an individual particle satisfies

$$m\frac{\mathrm{d}U_i}{\mathrm{d}t} = F_i, \qquad \frac{2}{5}ma^2\frac{\mathrm{d}\Omega_i}{\mathrm{d}t} = \mathscr{L}_i, \tag{2.3}$$

where U_i and Ω_i are, respectively, the translational and rotational velocities of the particle, t is the time, a is the radius of the particle, and F_i and $\mathscr{L}_i$ are the hydrodynamic force and torque exerted by the gas on the particle.

Finally, we assume that the continuum approximation given by (2.1) does not apply to the gas motion in the narrow gaps between particles separated by distances less than $2\epsilon_m a$. For such pairs of particles we evaluate F_i and $\mathscr{L}_i$ by taking the gap width to equal $2\epsilon_m a$. A relation between $\epsilon_m a$ and the mean free path λ of the gas molecules is given in §3.1.1. The collisions between the particles are assumed to be representative of smooth particles with a coefficient of restitution e.

Our goal is to calculate the velocity variance and particle-phase rheology as a function of $St = m\gamma/(6\pi\mu a)$, e, ϕ, and λ/a or equivalently ϵ_m.

3. Theory for $St \gg 1$ and $0 \leqslant 1 - e \ll 1$

The variance of the particle velocity at steady state is determined from the energy balance equation for the fluctuating motion of the particles. This energy balance can be derived using standard techniques of statistical mechanics, as is done in the rapid granular flow literature. Thus, the energy balance is given by (see, for example, Babic 1993)

$$\tfrac{3}{2}\rho_p\phi\frac{\mathrm{d}T}{\mathrm{d}t} = -\frac{\partial q_j}{\partial x_j} + \gamma_{ij}\sigma_{ij} - \Gamma, \tag{3.1}$$

where ρ_p is the density of the particle, T is the particle-phase temperature defined as one-third of the velocity variance with respect to the ensemble-averaged velocity $\langle U_i\rangle$, $\mathrm{d}/\mathrm{d}t = \partial/\partial t + \langle \boldsymbol{U}\rangle \cdot \nabla$ is the time derivative following the average motion, σ_{ij} is the particle-phase stress, q_j is the flux of fluctuation energy, and Γ is the rate of energy dissipation per unit volume of the suspension. We are interested in the present section in the case of large St (equivalent to a large viscous relaxation time) and nearly elastic particles. The effect of hydrodynamic interactions among particles is small at large St and the particles travel in nearly straight lines between successive collisions. Thus, the particles are expected to behave similarly to the molecules of a dense gas consisting of smooth, spherical molecules with a hard-sphere interaction potential. In dense-gas theory the temperature is multiplied by the Boltzmann constant to obtain a mechanical equivalent of heat while in the present case of gas–solid flows T is directly related to the internal kinetic energy of the suspension. We shall therefore use the standard expressions for the equation of state, viscosity, and conductivity of dense granular materials and write

$$\sigma_{ij} = -P\delta_{ij} + 2\mu_s e_{ij} + (\kappa - \tfrac{2}{3}\mu_s)e_{kk}\delta_{ij}, \tag{3.2}$$

$$q_j = -k\frac{\partial T}{\partial x_j}, \tag{3.3}$$

where

$$e_{ij} = \tfrac{1}{2}(\gamma_{ij} + \gamma_{ji}) \tag{3.4}$$

is the rate of strain tensor, P is the particle-phase pressure, μ_s and κ are, respectively, the coefficients of shear and bulk viscosity, and k is the pseudo-thermal conductivity. Using expressions from dense-gas theory, we write

$$P = \rho_p\phi T(1 + 4\phi\chi), \tag{3.5}$$

$$\mu_s = \frac{16}{5\pi^{1/2}}\rho_p a T^{1/2}\phi^2\chi\left[1 + \frac{\pi}{12}\left(1 + \frac{5}{8\phi\chi}\right)^2\right], \tag{3.6}$$

$$\kappa = \frac{16}{3\pi^{1/2}}\rho_p a T^{1/2}\phi^2\chi, \tag{3.7}$$

$$k = \frac{8}{\pi^{1/2}}\rho_p a T^{1/2}\phi^2\chi\left[1 + \frac{25\pi}{512\phi^2\chi^2}\right], \tag{3.8}$$

where χ is the value of the radial distribution function at $r = 2a$. For a hard-sphere distribution, a good approximation to its value for $\phi < 0.5$ is obtained from (Carnahan & Starling 1969)

$$\chi = \frac{1 - \phi/2}{(1-\phi)^3}. \tag{3.9}$$

The above results (3.5)–(3.9) are taken from a recent paper by Babic (1993) who has put the previously known results for the hard-sphere and hard-disk suspensions in a convenient tabulated form. The radial distribution for $\phi > 0.5$ can be estimated, for example, from the approximation χ^M given by Ma & Ahmadi (1988) or χ^W by Woodcock (1981):

$$\chi^M = \frac{1 + 2.5\phi + 4.590\phi^2 + 4.5904\phi^2 + 4.515439\phi^3}{[1 - (\phi/0.64356)^3]^{0.678021}}, \qquad \chi^W = \frac{1.2\phi}{[1 - (\phi/0.62)]}. \tag{3.10}$$

The total energy dissipation rate Γ is the sum of the energy dissipated due to inelastic collisions and that due to finite gas viscosity. The leading-order estimates of these can be obtained by assuming that the translational velocity distribution is an isotropic Maxwellian. This leads to the well-known estimate of the dissipation due to inelastic effects:

$$\Gamma_{inelas} = \frac{12}{a\pi^{1/2}}(1 - e)\rho_p\phi^2\chi T^{3/2}. \tag{3.11}$$

The rate of viscous energy dissipation in a suspension with a zero mean relative motion between the particles and the suspension is expressed in terms of T as

$$\Gamma_{vis} \equiv -n\langle \boldsymbol{F} \cdot (\boldsymbol{U} - \langle \boldsymbol{U} \rangle) + (\boldsymbol{\Omega} - \langle \boldsymbol{\Omega} \rangle) \cdot \mathscr{L} \rangle = 18\pi\mu a n T R_{diss}, \tag{3.12}$$

where n is the number density of the particles and the angular brackets denote average over all the particles in the suspension. Here, we have assumed that the magnitude of fluctuations in rotational velocity and torque are negligible. Note that the above expression for Γ_{vis} must be corrected for the dissipation arising from the affine motion when the mean relative motion is not zero (see Nott & Brady 1994 for a more complete expression for Γ_{vis}). We also note that R_{diss} may be interpreted as an effective drag coefficient of a sphere moving in a fixed bed of particles. The dissipation coefficient R_{diss} as a function of ϕ and ϵ_m will be determined in §3.1.

We now consider a homogeneous suspension at steady state. The mass conservation equation for the particle phase (cf. (4.13)) then requires $\gamma_{ii} = 0$ and the energy conservation equation subsequently reduces to

$$\Gamma_{inelas} + \Gamma_{vis} = \sigma_{ij}\gamma_{ij} = 2\mu_s e_{ij}\gamma_{ij} = \mu_s\gamma^2. \tag{3.13}$$

Note that for general shear we define γ through the last equality in (3.13). According to (3.13) the energy input in shearing a homogeneous suspension at steady state equals the energy dissipated by viscous and inelastic effects. Substituting (3.6), (3.11), and (3.12) into (3.13) for μ_s, Γ_{vis}, and Γ_{inelas}, respectively, yields a cubic equation for $T^{1/2}$, one root of which is negative and hence unphysical, and the other two roots correspond to $T = 0$ and

$$\frac{T^{1/2}}{\gamma a} = \frac{\pi^{1/2}R_{diss}}{8\phi\chi St(1 - e)}\left[\left\{1 + \frac{256\phi^2\chi^2}{15\pi}\frac{St^2}{R_{diss}^2}(1 - e)[1 + \frac{\pi}{12}(1 + \frac{5}{8\phi\chi})^2]\right\}^{1/2} - 1\right] \qquad (St \gg 1, \quad 0 < 1 - e \ll 1). \tag{3.14}$$

For the special case of elastic collisions ($e = 1$), the steady-state variance can be evaluated from

$$\frac{T^{1/2}}{\gamma a} = \frac{16}{15\pi^{1/2}}\frac{St}{R_{diss}}\phi\chi\left[1 + \frac{\pi}{12}\left(1 + \frac{5}{8\phi\chi}\right)^2\right] \qquad (e = 1, \quad St \gg 1). \tag{3.15}$$

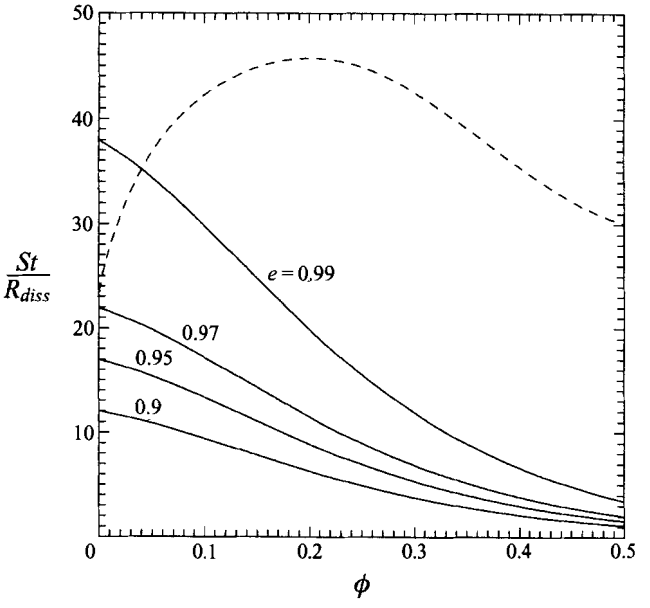

FIGURE 1. The value of St/R_{diss} for which the energy dissipations by viscous and inelasticity effects become equal in magnitude for various indicated values of the coefficient of restitution e. The dashed curve shows the value of St for $e = 0.97$ with R_{diss} determined from (3.18) and $a/\lambda = 500$.

When $\phi \ll 1$, the above reduces to

$$\frac{T^{1/2}}{\gamma a} = \frac{1}{16.248\ldots}\left(\frac{St}{R_{diss}\phi}\right) \qquad (\phi \ll 1,\ e = 1,\ St \gg 1), \tag{3.16}$$

in agreement with the result derived by Tsao & Koch (1995). The effect of viscous dissipation on the granular temperture of the suspension was also studied previously by Ma & Ahmadi (1988). These investigators used the Bhatnagar–Gross–Krook (BGK) relaxation model for evaluating the collision integral contribution to the average moments equation (cf. (4.8)). For small ϕ their analysis gave the constant of 12.58 instead of 16.248... in the above expression. Also their analysis suggested using the average drag coefficient based on the average hindrance factor in sedimenting suspensions in place of R_{diss} which represents the drag coefficient of a sphere suspended in a fixed bed of particles. The two drag coefficients, however, differ considerably at finite ϕ and one must use R_{diss} to correctly predict T.

Finally, we note that for suspensions with significant inertial effects, the state of homogeneous steady suspension cannot be maintained in general for arbitrary shear as can be seen from the momentum equation for the particle phase (cf. (4.14)). The inertial terms for an arbitrary imposed shear are generally balanced by the particle-phase stress gradient which can only occur when the gradients of volume fraction and T are non-zero. Thus, a more general analysis must account for linear variation in ϕ as well as T. In the limit of large St and small $1 - e$, for which $T/(\gamma^2 a^2)$ is very large, it can be shown, however, that the magnitude of the gradient in ϕ is small and so $\nabla \cdot \langle \boldsymbol{U} \rangle$ is small compared with the magnitude of $\nabla \langle \boldsymbol{U} \rangle$.

The predictions of the above asymptotic theory will be compared with the results of simulations in §5. In the next subsection we shall determine R_{diss}. However, first it is interesting to obtain a rough criterion for estimating the relative importance of viscous and inelastic effects. With T given by (3.14), we can determine the value of

St/R_{diss} for given ϕ and e at which $\Gamma_{vis} = \Gamma_{inelas}$. The results are shown in Figure 1. At small ϕ, the two effects are equal in magnitude when

$$(1-e)\frac{St^2}{R_{diss}^2} = \frac{72}{5} \qquad (\phi \ll 1) \tag{3.17}$$

and the value of St/R_{diss} monotonically decreases with ϕ. On the other hand, the actual value of St at which the two mechanisms cause an equal amount of dissipation can increase with ϕ, since the dissipation coefficient R_{diss} increases with ϕ. The dashed line in figure 1 shows St as a function of ϕ for $e = 0.97$ and $a/\lambda = 500$. Here, we have used the results for R_{diss} to be presented in the following subsection.

It should be noted that the criterion for the equality of viscous and inelastic dissipation rates based on the theory for $1-e \ll 1$ and $St \gg 1$ tends to underestimate the importance of viscous stresses. For example, viscous dissipation is essential to give the multiplicity of steady states observed by Tsao & Koch (1995) for low volume fractions. In addition, Tsao & Koch (1995) showed that the nonlinear drag arising at finite Reynolds numbers tends to increase the importance of hydrodynamics relative to inelasticity. However, one important conclusion from the comparison of the two dissipation mechanisms is that for suspensions in which ϕ is not too small, significant viscous effects will occur primarily when St/R_{diss} is $O(1)$. Thus, it will be necessary to develop a theory for that case. This will be done in §4.

3.1. *Determination of* R_{diss}

As mentioned earlier, we must estimate the rate of energy dissipation in a suspension in which the particles have a hard-sphere spatial and velocity distribution in the limit of small $1-e$ and large St. For this purpose, we used the usual hard-sphere molecular dynamics code in which N particles were placed in a periodic unit cell and given random velocities with zero mean. In other words, the trajectories of the particles were determined by neglecting the viscous forces and the collision rules were based on perfectly elastic collisions. Each sphere was allowed to undergo several thousand collisions and the positions and velocities of the particles were stored at regular time intervals for later use in hydrodynamic calculations as described in the following paragraph.

R_{diss} was determined by solving the Stokes equations of motion for flow around particles with their positions and translational velocities given by the molecular-dynamics code described above. The rotational velocities of the particles were taken to be zero in these calculations. In a suspension of smooth, frictionless spheres, the solid-body collisions do not drive particle rotations. Thus, fluctuations in the rotational velocity in a sheared suspension will result only from hydrodynamic torques and, at least in a weakly dissipative system for which $T \gg \gamma^2 a^2$, the rotational velocity fluctuations (multiplied by a) will be small compared with the translational velocity fluctuations. The Stokes flow interactions among particles were computed using the method described in Mo & Sangani (1994) and Sangani & Mo (1994). The velocity was expressed in terms of point forces and force dipoles at the centres of the particles and lubrication force dipoles at the centre of the gap between close particles. As shown in these papers, the method gives an accuracy that is comparable to that obtained by the methods of Brady & Bossis (1988) and Ladd (1990).

Results for R_{diss} as a function of ϕ for several different values of ϵ_m are shown in figure 2. These results are obtained by averaging over 100 configurations with $N = 54$ for each ϕ and ϵ_m. As one would expect, R_{diss} increases with increasing ϕ and decreasing ϵ_m. The variation of R_{diss} with ϵ_m for $\phi = 0.15$ and $\phi = 0.5$ is shown in

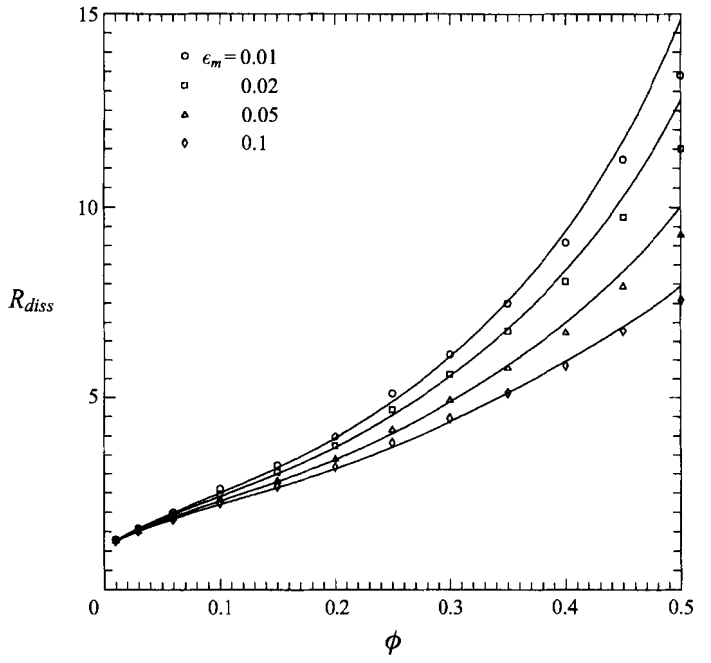

FIGURE 2. R_{diss} as a function of ϕ and ϵ_m. The solid lines represent the values obtained from (3.18) using (3.22) and (3.24).

Figure 3. It is clear that R_{diss} diverges logarithmically with ϵ_m. Thus, we fit our results for different values of ϕ and ϵ_m according to

$$R_{diss} = k_1(\phi) - k_2(\phi) \ln \epsilon_m \tag{3.18}$$

and plot k_1 and k_2 as functions of ϕ in figures 4 and 5.

The logarithmic divergence of R_{diss} with ϵ_m results from the energy dissipation due to the lubrication flows in the narrow gaps between particles and therefore it is relatively straightforward to obtain an analytical expression for k_2. The viscous energy dissipation can be expressed in terms of the two-particle probability distribution f_2 by means of an integral

$$\Gamma_{vis} = -n\langle \boldsymbol{F} \cdot \boldsymbol{C} \rangle = -\int (\boldsymbol{F} \cdot \boldsymbol{C}) f_2(\boldsymbol{C}, \boldsymbol{C}_1, \boldsymbol{r}, \boldsymbol{0}) \mathrm{d}\boldsymbol{C} \mathrm{d}\boldsymbol{C}_1 \mathrm{d}\boldsymbol{r}, \tag{3.19}$$

where $\boldsymbol{F}$ is the force exerted by the gas on a test particle with velocity $\boldsymbol{C}$ placed at $\boldsymbol{0}$ in the presence of another particle with velocity $\boldsymbol{C}_1$ at $\boldsymbol{r}$. We assume that the velocities of the particles are uncorrelated and satisfy the Maxwellian distribution

$$f_M(\boldsymbol{C}) = \frac{n}{(2\pi T)^{3/2}} \exp\left(-\frac{C^2}{2T}\right), \tag{3.20}$$

and take $f_2 = f_M(\boldsymbol{C}) f_M(\boldsymbol{C}_1) P(\boldsymbol{r}|\boldsymbol{0})$, P being the pair probability distribution for the hard-sphere spatial distribution normalized by the number density n. For small particle separations $2a\epsilon_m < r - 2a \ll a$, $\boldsymbol{F}$ is given by (see, for example, Kim & Karrila 1991, chap. 9)

$$\boldsymbol{F} = -6\pi\mu \boldsymbol{r}(\boldsymbol{C} - \boldsymbol{C}_1) \cdot \boldsymbol{r} \frac{1}{8(r - 2a)}, \tag{3.21}$$

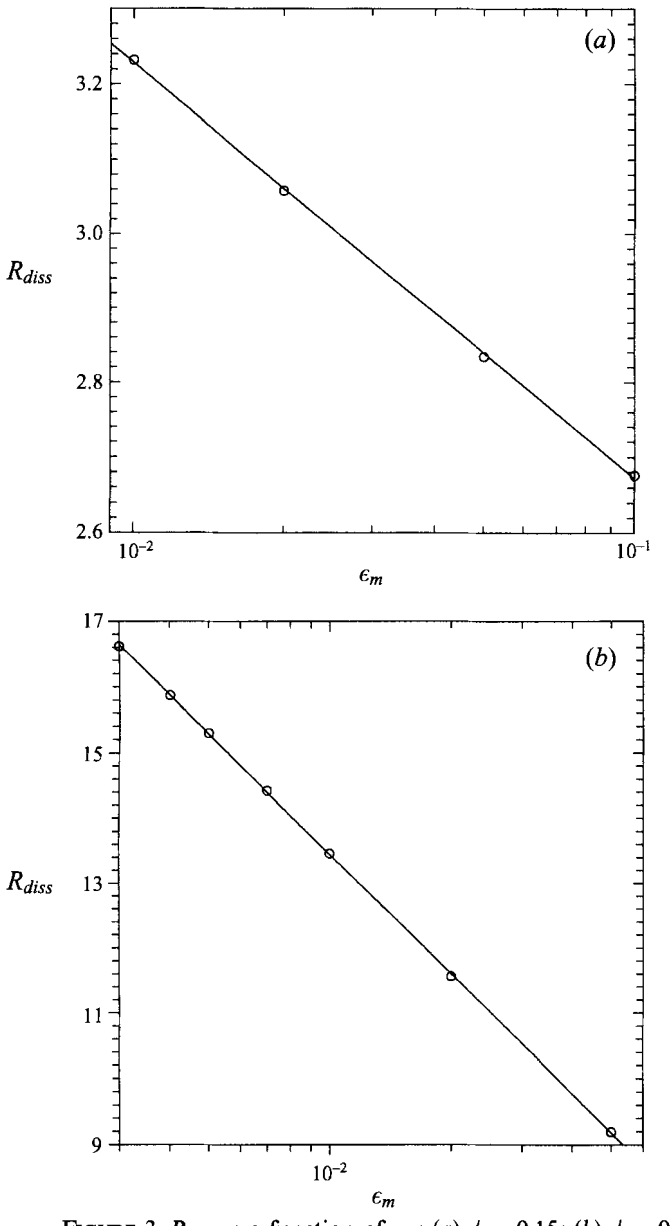

FIGURE 3. R_{diss} as a function of ϵ_m: (*a*) $\phi = 0.15$; (*b*) $\phi = 0.5$.

and hence upon substituting for f_2 and $\boldsymbol{F}$, and performing the integration in (3.19), it is easy to show that the logarithmically divergent part of Γ_{vis} is simply given by

$$k_2(\phi) = \phi\chi, \tag{3.22}$$

where χ equals the radial distribution function at $r = 2a$. Since in this asymptotic limit of large St and small $1 - e$, the particle configurations resemble the hard-sphere molecular system, we shall use the Carnahan–Starling approximation (cf. (3.9)) for χ. The solid curve in figure 5 represents the above result with χ given by (3.9) while the circles represent the values of k_2 obtained by fitting the numerical results for R_{diss}. The agreement between the two is excellent for all values of ϕ except at $\phi = 0.5$

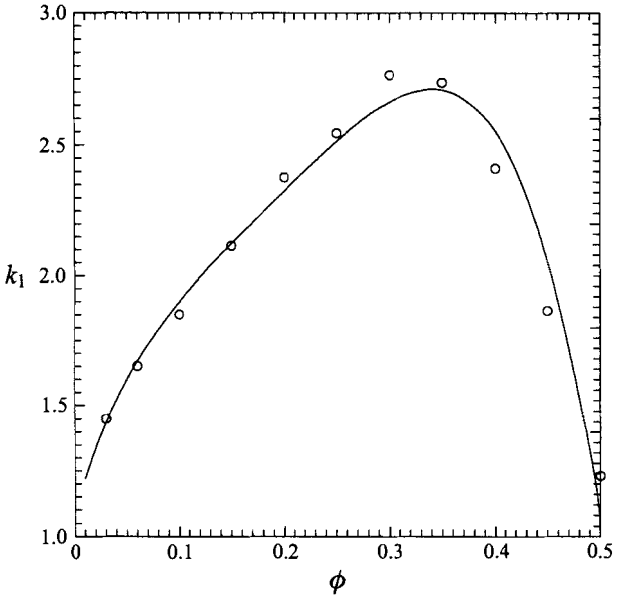

FIGURE 4. k_1 as a function of ϕ. The circles are obtained by fitting the computed results for R_{diss} according to (3.18) while the solid line represents (3.24).

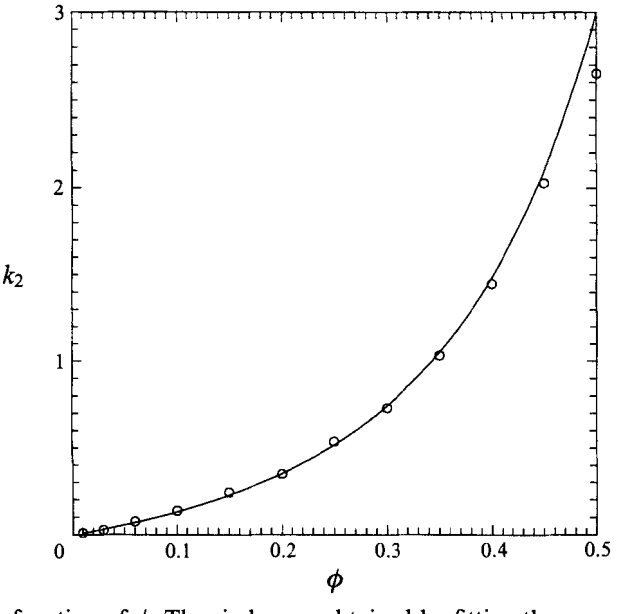

FIGURE 5. k_2 as a function of ϕ. The circles are obtained by fitting the computed values of R_{diss} according to (3.18) while the solid line represents (3.22) with χ determined from the Carnahan–Starling approximation (3.9).

for which the computed value of χ, i.e. k_2/ϕ, is lower than that predicted by (3.9) or (3.10): the computed value of χ from the numerical results for k_2 is 5.3 while the Carnahan–Starling, Ma & Ahmadi, and Woodcock expressions (cf. (3.9) and (3.10)) give the respective estimates of 6.0, 6.1, and 6.2. The reason for this discrepancy is the small system size ($N = 54$) used in our simulations. To show this, we carried

out calculations for the collision frequency in the hard-sphere system with $e = 1$ and $St = \infty$ at $\phi = 0.5$ for $N = 54$ and $N = 108$. Assuming the Maxwellian velocity distribution, χ is estimated from the collision frequency in simulations by means of

$$\chi^S = \frac{a\pi^{1/2}\dot{N}_c}{3NT^{1/2}} \tag{3.23}$$

where $\dot{N}_c$ is the rate of collisions. The numerical simulations for $N = 54$ and 108 gave χ^S of respectively 5.4 and 5.9, the latter being in good agreement with the Carnahan–Starling approximation.

The results for k_1 are best fitted by the expression

$$k_1(\phi) = 1 + \frac{3}{\sqrt{2}}\phi^{1/2} + \frac{135}{64}\phi\ln\phi + 11.26\phi(1 - 5.1\phi + 16.57\phi^2 - 21.77\phi^3). \tag{3.24}$$

The terms up to $O(\phi\ln\phi)$ in the above expression are the same as in the expression for the average force on a particle in a fixed bed of particles in the presence of a mean fluid flow (see, for example, Howells 1974; Hinch 1977; Kim & Russell 1985) because the far-field velocity disturbances in both problems are similar and governed by Brinkman screening. The coefficients of the higher-order terms in (3.24) are obtained by curve fitting the numerical results for R_{diss}. It is interesting to note that k_1 goes through a maximum near $\phi = 0.35$ so that the numerical values of k_1 vary over a rather narrow range from 1 to about 2.8. Thus, in very dense suspensions R_{diss} is completely dominated by lubrication forces. Since the hydrodynamic interactions in suspensions with the velocity of the particles specified are governed by the Brinkmann screening at large distances from a test sphere, k_1 is expected to be relatively insensitive to the system size N (see, for example, Ladd 1990).

A comparison between the computed values of R_{diss} and those obtained by using (3.18), with k_1 and k_2 evaluated from (3.24) and (3.22), is shown in figure 2. The agreement is seen to be very good except at $\phi = 0.5$, where, as mentioned earlier, our computed value of χ (or k_2) differs from that given by (3.9) owing to small number of particles used in simulations.

3.1.1. *A relation between λ and ϵ_m*

We close this section by noting a relation between the mean free path λ of the gas molecules and the lubrication cut-off $a\epsilon_m$ used in our model for viscous dissipation. Our calculations for R_{diss} assumed that the standard lubrication approximations for rigid, smooth spherical particles in Stokes flow break down when the gap width between the particles become comparable to $2\epsilon_m a$. There are a number of mechanisms for the breakdown of standard lubrication approximation, e.g. the roughness of the particles (Smart & Leighton 1989) and the finite compressibility of the particles (see Barnocky & Davis 1989 and references therein), and in principle it is possible to relate ϵ_m to the appropriate parameter responsible for the lubrication breakdown. The mean free path of a gas at standard atmospheric pressure and temperature is about 0.1 μm while the low-Re, finite-St approximation is likely to apply for a in the range of 10–100 μm. For particles with roughness smaller than λ, we expect λ/a to be the most important parameter in determining ϵ_m.

Sundararajakumar & Koch (1996) have recently examined in detail the motion of the gas in the narrow region between two smooth, rigid spherical particles approaching one another. Their analysis accounts for the finite mean free path λ of the gas molecules and calculates the force on each particle as a function of the gap width between the particles. By comparing the total energy dissipated as two particles with

high St approach each other with the corresponding energy dissipated in our model we find that

$$a\epsilon_m = 4.88\lambda \qquad (St \gg 1). \tag{3.25}$$

4. Approximate theory for moderately large St/R_{diss} and $(1-e)^{-1}$

The theory presented in §3 is asymptotically valid in the limits $St \gg 1$ and $1-e \ll 1$. However, it takes no account of the deviations from Newtonian rheology and the resulting effects on the energy balance that occur for more moderate values of St and $1-e$. Lun *et al.* (1984) have developed a theory using a moment approach to determine the first effects of finite particle inelasticity on the rheology of a granular material. We will adopt a similar approach to determine the combined effects of finite St and $1-e$ on the moments of the velocity distribution. This approach will not be applicable to Stokes numbers smaller than about 2, which may be encountered in liquid–solid suspensions. However, the case of purely viscous suspensions at $St = 0$ has already been extensively studied analytically (see a review by Brady & Bossis 1988) as well as experimentally (e.g. Gadala-Maria & Acrivos 1980).

Let $f(t, x_i, U_i, \Omega_i)$ be the one-particle probability distribution function normalized such that

$$\int \mathrm{d}\boldsymbol{U}\mathrm{d}\boldsymbol{\Omega} f(t, x_i, U_i, \Omega_i) = n(t, x_i), \tag{4.1}$$

where $n(t, x_i)$ is the number density of particles. Then f satisfies the usual conservation equation

$$\frac{\partial f}{\partial t} + U_i \frac{\partial f}{\partial x_i} + \frac{\partial}{\partial U_i}(\dot{U}_i f) + \frac{\partial}{\partial \Omega_i}(\dot{\Omega}_i f) = \frac{\partial_c f}{\partial t}, \tag{4.2}$$

where $\dot{U}_i$ represents the acceleration of the particle due to body and viscous forces acting on it and $\partial_c f/\partial t$ represents the rate of change of the number of particles with velocity U_i at point x_i due to collisions. It is convenient to introduce the fluctuation velocity C_i of the particle defined by

$$C_i = U_i - \langle U_i \rangle(x_i), \tag{4.3}$$

where $\langle U_i \rangle = (1/n)\int f U_i \mathrm{d}\boldsymbol{U}$ is the average velocity of the particles. Since the fluctuations in the rotational velocities of the particles at finite St as determined from the direct numerical simulations (§5) do not appear to be significant, we shall neglect the influence of the rotational degree of freedom of the particles. Thus, the conservation equation for f in terms of (t, x_i, C_i) is written as (see Chapman & Cowling 1970)

$$\frac{\mathrm{d}f}{\mathrm{d}t} - \frac{\mathrm{d}\langle U_k \rangle}{\mathrm{d}t}\frac{\partial f}{\partial C_k} + C_j \frac{\partial f}{\partial x_j} - C_m \gamma_{km} \frac{\partial f}{\partial C_k} + \frac{\partial}{\partial C_j}(\dot{U}_j f) = \frac{\partial_c f}{\partial t}. \tag{4.4}$$

For hard-sphere systems, the collisional contribution appearing on the right-hand side of (4.4) can be expressed in terms of an integral first used in the study of dense gases by Enskog (see Chapman & Cowling 1970, chap. 16, and Lun *et al.* 1984 for a formal derivation):

$$\frac{\partial_c f}{\partial t} = \int_{\boldsymbol{g}\cdot\boldsymbol{k}>0} [\chi(\boldsymbol{x}+a\boldsymbol{k}) f(\boldsymbol{C}', \boldsymbol{x}) f(\boldsymbol{C}_1', \boldsymbol{x}+2a\boldsymbol{k}) - \chi(\boldsymbol{x}-a\boldsymbol{k}) f(\boldsymbol{C}, \boldsymbol{x}) f(\boldsymbol{C}_1, \boldsymbol{x}-2a\boldsymbol{k})] \times 4a^2 \boldsymbol{g}\cdot\boldsymbol{k}\mathrm{d}\boldsymbol{k}\mathrm{d}\boldsymbol{C}_1, \tag{4.5}$$

where, for the sake of brevity, we have suppressed the explicit dependence of χ and

f on time. Here, χ is the value of the radial distribution function at $r = 2a$. Note that for inhomogeneous suspensions, in which ϕ is varying with position, the radial distribution function is also a function of position. Equation (4.5) accounts for both the rate of decrease in the probability density for a particle with (fluctuation) velocity $\boldsymbol{C}$ centred at $\boldsymbol{x}$ due to a collision with a particle centred at $\boldsymbol{x} - 2a\boldsymbol{k}$ whose velocity is $\boldsymbol{C}_1$, and the rate of increase due to an 'inverse' collision in which the two particles with relative velocities $\boldsymbol{C}'$ and $\boldsymbol{C}_1'$, centred respectively at $\boldsymbol{x}$ and $\mathbf{x} + 2a\boldsymbol{k}$, collide resulting in particles with relative velocities $\boldsymbol{C}$, and $\boldsymbol{C}_1$ after the collision. Here, $\boldsymbol{k}$ is a unit vector,

$$\boldsymbol{g} = \boldsymbol{C}_1 - \boldsymbol{C} - 2a\gamma\cdot\boldsymbol{k}, \quad \boldsymbol{C}' = \boldsymbol{C} + \eta(\boldsymbol{k}\cdot\boldsymbol{g})\boldsymbol{k}, \quad \boldsymbol{C}_1' = \boldsymbol{C}_1 - \eta(\boldsymbol{k}\cdot\boldsymbol{g})\boldsymbol{k}, \quad \eta = (1+e)/2. \tag{4.6}$$

The factor $\chi(\boldsymbol{g}\cdot\boldsymbol{k})$ is proportional to the frequency with which collisions occur between particles with velocity $\mathbf{C}$ and $\boldsymbol{C}_1$. It may be noted that for dilute suspensions, $\chi \approx 1$ and $f(\boldsymbol{x} \pm 2a\boldsymbol{k}) \approx f((\boldsymbol{x})$, so that the above integral reduces to the well-known Boltzmann integral.

In writing (4.5), we have assumed that the two-particle probability distribution $f_2(\boldsymbol{C}, \boldsymbol{C}_1, \boldsymbol{x}, \boldsymbol{x} - 2a\boldsymbol{k})$ can be approximated as the product of single-particle distributions. This is known as the molecular chaos approximation and is a widely accepted approximation in the granular flow literature (see e.g. Lun *et al.* 1984). In general, the two-particle distribution function will be affected by the hydrodyanamic interactions between the particles before they actually come into contact. For large St, this effect will be small (Koch 1990). We found in our numerical simulations that there was no noticeable deviation of the radial distribution function value at $r \approx 2a$ for $St/R_{diss} > 2$ and we thereby concluded that the effects of hydrodynamic interactions on the two-particle encounter were weak even at this moderate value of St/R_{diss}.

Let $\psi(\boldsymbol{C})$ be any dynamic variable associated with the particle motion and define $\langle\psi\rangle$ by

$$n\langle\psi\rangle = \int f\psi \mathrm{d}\boldsymbol{C}. \tag{4.7}$$

A balance equation for $\langle\psi\rangle$ is obtained by multiplying (4.4) with $\psi d\boldsymbol{C}$ and integrating:

$$\langle\psi\rangle\left[\frac{\mathrm{d}n}{\mathrm{d}t} + n\gamma_{kk}\right] + n\left[\frac{\mathrm{d}\langle\psi\rangle}{\mathrm{d}t} + \frac{\mathrm{d}\langle U_k\rangle}{\mathrm{d}t}\langle\frac{\partial\psi}{\partial C_k}\rangle + \gamma_{km}\langle C_m\frac{\partial\psi}{\partial C_k}\rangle - \langle\dot{U}_k\frac{\partial\psi}{\partial C_k}\rangle\right] = n\frac{\partial_c\langle\psi\rangle}{\partial t}, \tag{4.8}$$

where

$$n\frac{\partial_c\langle\psi\rangle}{\partial t} \equiv \int \psi\frac{\partial_c f}{\partial t}\mathrm{d}\boldsymbol{C}. \tag{4.9}$$

Assuming that χ and f vary on a length scale large compared to a, the right-hand side of (4.5) can be expanded in a Taylor series near $\boldsymbol{x}$, and neglecting terms of third and higher order in a, it can be shown that (see Jenkins & Richman 1985 and Kremer & Rosa 1988 for details)

$$n\frac{\partial_c\langle\psi\rangle}{\partial t} = S(\psi) - \frac{\partial}{\partial x_k}Q_k(\psi) - \gamma_{kl}Q_l\left(\frac{\partial\psi}{\partial C_k}\right), \tag{4.10}$$

where

$$S(\psi) = \chi\int_{\boldsymbol{g}\cdot\boldsymbol{k}>0}(\psi - \psi')f(\boldsymbol{C})f(\boldsymbol{C}_1)\left\{1 + a\boldsymbol{k}\cdot\nabla\ln\frac{f(\boldsymbol{C})}{f(\boldsymbol{C}_1)}\right\}(4a^2)(\boldsymbol{g}\cdot\boldsymbol{k})\mathrm{d}\boldsymbol{C}\mathrm{d}\boldsymbol{C}_1\mathrm{d}\boldsymbol{k}, \tag{4.11}$$

$$\boldsymbol{Q}(\psi) = a\chi \int_{\boldsymbol{g}\cdot\boldsymbol{k}>0} (\psi' - \psi)\boldsymbol{k} f(\boldsymbol{C}) f(\boldsymbol{C}_1) \left\{1 + a\boldsymbol{k}\cdot\nabla \ln \frac{f(\boldsymbol{C})}{f(\boldsymbol{C}_1)}\right\} (4a^2)(\boldsymbol{g}\cdot\boldsymbol{k}) \mathrm{d}\boldsymbol{C}\mathrm{d}\boldsymbol{C}_1\mathrm{d}\boldsymbol{k}. \tag{4.12}$$

Here χ and f are evaluated at $\boldsymbol{x}$, and ψ' is the value of ψ just after the collision. The assumption that f varies slowly with position is strictly valid only for $T \gg \gamma^2 a^2$, but we will see that this expansion gives results that are in good agreement with simulations even at moderate values of St/R_{diss} for $\phi = O(1)$.

The mass, momentum, and energy equations for the particle-phase motion can now be derived by taking ψ to equal, respectively, m, $m\boldsymbol{C}_i$ and $mC^2/2$. Using $mn = \rho_p\phi$, the mass conservation equation is given by

$$\rho_p \frac{\mathrm{d}\phi}{\mathrm{d}t} + \rho_p \phi \gamma_{kk} = 0. \tag{4.13}$$

The momentum conservation equation is given by

$$\rho_p \phi \frac{\mathrm{d}\langle U_i\rangle}{\mathrm{d}t} = \frac{\partial}{\partial x_j}(\sigma_{ij}^k + \sigma_{ij}^c) + \rho_p \phi \langle \dot{U}_i\rangle, \tag{4.14}$$

where

$$\sigma_{ij}^k = -\rho_p \phi \langle C_i C_j\rangle, \qquad \sigma_{ij}^c = -mQ_j(C_i) \tag{4.15}$$

are the usual kinetic and collisional contributions to the stress. Note that $S(C_i) = 0$ since momentum is conserved during the collisions.

The last term on the right-hand side of (4.14) can be expressed as

$$\rho_p \phi \langle \dot{U}_i\rangle = -6\pi\mu a n R_{drag}\langle U_i - u_i\rangle + \frac{\partial \sigma_{ij}^h}{\partial x_j}, \tag{4.16}$$

where $\langle u_i\rangle$ is the average velocity of the suspension, R_{drag} is the average drag coefficient and σ_{ij}^h is the contribution to the particle-phase stress due to hydrodynamic interactions among particles. For zero Stokes number suspensions this stress is related to the average stresslet induced by the presence of the particles. For finite Stokes numbers there is an additional contribution arising from the hydrodynamic interactions which roughly speaking can be expressed as $\langle x_i^\alpha F_j^\alpha\rangle$, F_j^α being the force on particle α due to hydrodynamic interactions (see Nott & Brady 1994 for the formal expression for this stress). Calculation of this contribution to the stress in bubbly liquids has been addressed in recent publications (Sangani & Didwania 1993; Zhang & Prosperetti 1994; Bulthuis, Prosperetti & Sangani 1995). However, since this stress is $O(St^{-1})$, small compared to kinetic and collisional stresses, and since we are most interested in moderate to high St in the present study, we will neglect the contribution from the hydrodynamic stress. Finally, the energy equation is given by (3.1) with

$$q_j = \tfrac{1}{2}\rho_p\phi\left[\langle C^2 C_j\rangle + \tfrac{1}{n}Q_j(C^2)\right], \qquad \Gamma = -\tfrac{1}{2}mS(C^2) - mn\langle \dot{U}_j C_j\rangle = \Gamma_{inelas} + \Gamma_{vis}. \tag{4.17}$$

To determine T in a steady shear, we must solve for f and σ_{ij}. We shall adopt an approximate method developed by Grad (1949) to accomplish this. According to this method, f in a homogeneous suspension is assumed to be given by

$$f(\boldsymbol{C}) = \left\{1 + \tfrac{1}{2}T a_{ij}\frac{\partial^2}{\partial C_i \partial C_j}\right\} f_M, \tag{4.18}$$

where f_M is the isotropic Maxwellian distribution given by (3.20). It is easy to show that

$$\langle C_i C_j\rangle = \frac{1}{n}\int \mathrm{d}\boldsymbol{C} f(\boldsymbol{C}) C_i C_j = T(\delta_{ij} + a_{ij}). \tag{4.19}$$

Thus, a_{ij} is related to the second moments of the velocity distribution. Note also that, with T defined as one-third the particle velocity variance, $a_{ii} = 0$.

To determine a_{ij}, we substitute C_iC_j for ψ in (4.8) to obtain, in a steady homogeneous suspension,

$$\gamma_{ik}\langle C_kC_j\rangle + \gamma_{jk}\langle C_iC_k\rangle + \frac{2R_{diss}}{\tau_v}\langle C_iC_j\rangle = \frac{1}{n}S(C_iC_j) - \frac{1}{n}\{\gamma_{ik}Q_k(C_j) + \gamma_{jk}Q_k(C_i)\}, \quad (4.20)$$

where $\tau_v = m/(6\pi\mu a)$. In writing the last term on the left-hand side of (4.20) we have assumed that $\langle(\delta_{ik}C_j + \delta_{jk}C_i)\dot{U}_k\rangle = -(2/\tau_v)R_{diss}\langle C_iC_j\rangle$, which implicitly assumes (i) that the suspension microstructure is nearly isotropic even at finite St, and that (ii) R_{diss} determined in the limit of $St \to \infty$ with the hard-sphere velocity distribution is applicable even for finite Stokes number suspensions. Substituting for f from (4.18) into (4.11) and (4.12) yields the following expressions for S and $\boldsymbol{Q}$ (Jenkins and Richman 1985):

$$\frac{1}{n}S(C_iC_j) = -\frac{48}{5\pi^{1/2}a}\phi\chi\eta T^{3/2}\left[(2-\eta)a_{ij} + \tfrac{5}{3}(1-\eta)\delta_{ij}\right] + \tfrac{24}{5}\phi\chi\eta T\left[(3-2\eta)e_{ij} - (\eta - \tfrac{2}{3})e_{kk}\delta_{ij}\right], \quad (4.21)$$

$$\frac{1}{n}Q_i(C_j) = \eta\left[4\phi\chi T(\delta_{ij} + \tfrac{2}{5}a_{ij}) - \frac{32}{5\pi^{1/2}}\phi\chi aT^{1/2}(e_{ij} + \tfrac{1}{2}e_{kk}\delta_{ij})\right], \quad (4.22)$$

where $\eta = (1+e)/2$. The expressions above for S and $\mathbf{Q}$ neglect terms that are quadratic or higher order in a_{ij} and γ_{ij}. The theory of Tsao & Koch (1994) for dilute suspensions in the ignited state neglected terms that depend on e_{ij} and set $\boldsymbol{Q} = \mathbf{0}$ but included instead a term of $O(a_{ij}^2)$ in the expression for S. Their calculations suggest that keeping this quadratic term results in only minor numerical differences in the final results for the particle velocity variance and other average quantities. Tsao & Koch also constructed an approximate expression for S to account for the observed multiple steady states by including a term of $O(\gamma^3)$ corresponding to the leading behaviour of S in the quenched state. (Recall that $T \ll \gamma^2a^2$ for the quenched state.) The consequences of the different expressions for S in the theory presented here and that of Tsao & Koch will be discussed in more detail later.

Substituting for S and $\mathbf{Q}$ in (4.20), and rearranging, we obtain

$$e_{ij}\left[1 + \tfrac{4}{5}\phi\chi\eta(6\eta - 4)\right] + \frac{24}{5a\pi^{1/2}}\phi\chi\eta T^{1/2}\left[(2-\eta)a_{ij} + \tfrac{5}{3}(1-\eta)\delta_{ij}\right] + \tfrac{1}{2}\left[\gamma_{ik}a_{kj} + \gamma_{jk}a_{ki}\right](1 + \tfrac{8}{5}\phi\chi\eta) + \tfrac{R_{diss}}{\tau_v}(\delta_{ij} + a_{ij}) - \frac{16}{5\pi^{1/2}}\phi\chi a\eta T^{-1/2}[\gamma_{ik}e_{jk} + \gamma_{jk}e_{ki} + e_{kk}e_{ij}] + \tfrac{12}{5}\phi\chi\eta(\eta - \tfrac{2}{3})e_{kk}\delta_{ij} = 0. \quad (4.23)$$

The above equation together with the condition $a_{ii} = 0$ is sufficient to determine a_{ij} and T. A general solution to this equation for arbitrary shear is difficult and therefore we shall now consider the special case of simple shear with $e = 1$.

4.1. *Simple shear flow of perfectly elastic particles*

To test the validity of the above approximate theory, we shall compare its predictions to the results obtained from numerical simulations in §5. The simulations with periodic boundary conditions are easy to carry out for the case of simple shear for which

$$\gamma_{ij} = \gamma\delta_{i1}\delta_{j2}. \quad (4.24)$$

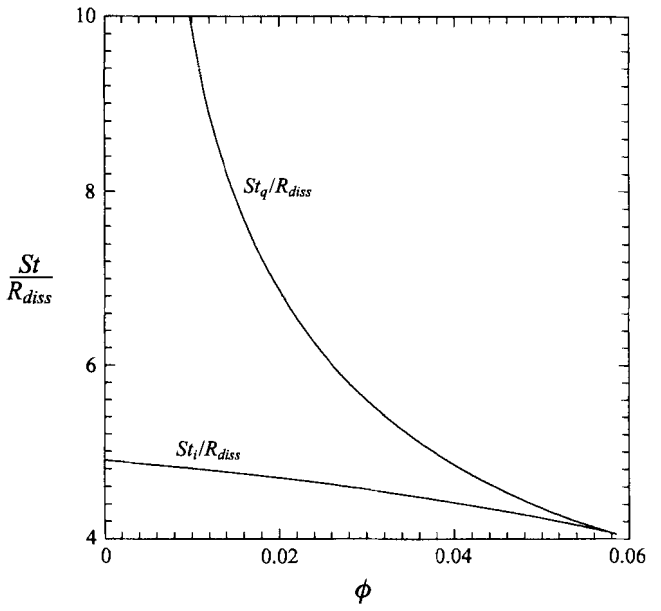

FIGURE 6. The critical Stokes numbers as functions of ϕ. The quenched state exists only for $St < St_q$ while the ignited state exists only for $St > St_i$.

To keep the resulting algebra somewhat less tedious, and to facilitate a detailed examination of the viscous effects, we shall first consider the case of elastic particles, i.e. $e = 1$. The case of inelastic particles with finite St will be considered separately in §6.

Substituting for γ_{ij} from (4.24) into (4.23), taking $\eta = 1$, and solving the resulting equations together with $a_{ii} = 0$ yields $a_{23} = a_{13} = 0$ and

$$a_{22} = a_{33} = -\tfrac{1}{2}a_{11} = -\frac{1}{1+\omega\overline{St}}, \tag{4.25}$$

$$a_{12} = -\frac{1}{2}\frac{\omega\overline{St}^2}{(1+\omega\overline{St})^2}(1+\tfrac{8}{5}\phi\chi), \tag{4.26}$$

$$\omega^3 + \omega^2\left[2\overline{St}^{-1} - \tfrac{1}{6}\overline{St}(1+\tfrac{8}{5}\phi\chi)^2 - \frac{128}{25\pi}\overline{St}\phi^2\chi^2\right] + \omega\left[\overline{St}^{-2} - \frac{256}{25\pi}\phi^2\chi^2\right] - \frac{128}{25\pi}\phi^2\chi^2\overline{St}^{-1} = 0, \tag{4.27}$$

where

$$\omega = \frac{24}{5\pi^{1/2}}\phi\chi\frac{T^{1/2}}{\gamma a}, \qquad \overline{St} = \frac{\gamma\tau_v}{R_{diss}} = \frac{St}{R_{diss}}. \tag{4.28}$$

Equation (4.27) is a cubic equation for ω, or equivalently $T^{1/2}$, and has therefore three roots. Only one root is real at very high $\overline{St}$. $T^{1/2}$ corresponding to this root asymptotically approaches (3.15) found in §3. The particle velocity variance is very large and therefore the collision time is much smaller than the viscous relaxation time. Thus, this root corresponds to the ignited state in the theory of Tsao & Koch (1994). This root is real and positive only for $\overline{St} > \overline{St}_i$, where $\overline{St}_i$ as a function of ϕ is given in figure 6. As $\phi \to 0$, $\overline{St}_i \to \sqrt{24} = 4.8989\ldots$ in agreement with the theory

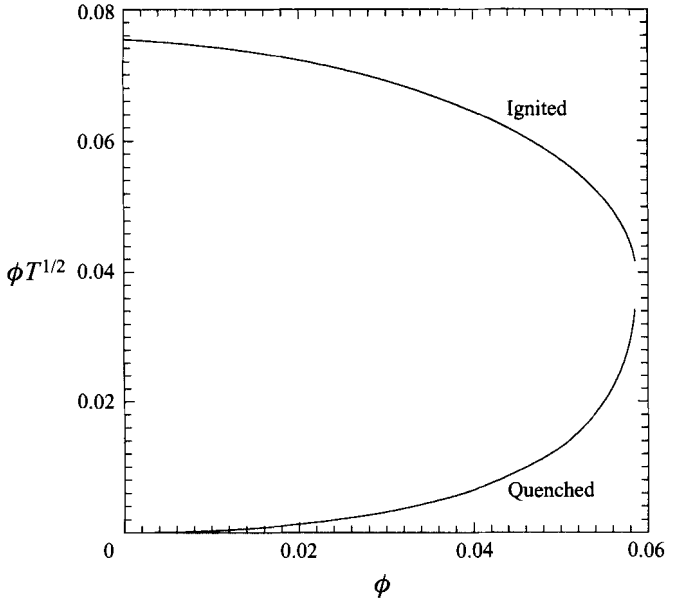

FIGURE 7. The value of $\phi T^{1/2}$ (non-dimensionalized by γa) for the quenched and ignited states at $St = St_i$

of Tsao & Koch (1994). (More exact calculations for the ignited state by including a term of $O(a_{ij}^2)$ in (4.21) resulted in $\overline{St}_i = \sqrt{171/7} = 4.9425\ldots$.) For very small values of $\overline{St}$, once again there is only one real positive root and since the velocity variance corresponding to this root is small, this is referred to as the quenched state. This root exists only for $\overline{St} < \overline{St}_q$, with $\overline{St}_q$ as a function of ϕ shown in figure 6. For small ϕ, this critical Stokes number is given by $\phi\overline{St}_q^2 = (75\pi/256)^{1/2} \approx 0.96$. For $\phi < 0.058$, we find that $\overline{St}_q > \overline{St}_i$ so that for such low volume fractions we have three real roots for $\overline{St}_i < \overline{St} < \overline{St}_q$ and the final steady-state variance depends on the initial conditions: if the initial variance is sufficiently small, the final state is quenched; otherwise the final state is ignited. As shown by Tsao & Koch (1994), the third root, whose variance is intermediate between the quenched and ignited states, is unstable so that it will not be observed in numerical simulations. Finally, for a fixed value of ϕ, the steady-state variance will abruptly change at $\overline{St} = \overline{St}_i$ from its value for the ignited state to that for the quenched state provided that $\phi < 0.058$. Figure 7 shows the magnitudes of $T^{1/2}$ for the quenched and ignited states at $\overline{St} = \overline{St}_i$ where this sudden jump in the variance will occur. The jump in variance is seen to vanish at $\phi \approx 0.058$.

According to the theory presented here $\phi\overline{St}_q^2 \approx 0.96$, and hence the conditions for observing multiple steady states are $\overline{St} > \overline{St}_i$ and $\phi\overline{St}^2 < 0.96$. Tsao & Koch (1994) obtained instead an approximate criterion $\phi St^3 < 3.23$. (Their numerical simulations without hydrodynamic interactions gave a more precise estimate of the numerical coefficient to be 1.5 instead of 3.23.) This and the magnitude the quenched-state variance in the two theories differ because of the different estimates of $S(C_iC_j)$ (cf. (4.21)) used in the two theories. As mentioned following (4.21), the term of $O(T^{3/2})$ in the expression for S which dominates in the ignited state is the same in both theories but, whereas we have a correction of $O(\gamma T)$, the theory of Tsao & Koch has the correction of $O(\gamma^3)$, which we neglected by assuming that the distribution function

varied slowly with position in (4.11). For dilute suspensions in the quenched state $T \ll \gamma^2 a^2$, and hence the criterion derived by Tsao & Koch is correct as $\phi \to 0$. Finally, we may add here that since our theory does not account for the additional contributions of $O(\gamma^3)$ in S, our estimate of $\phi = 0.058$ for the quenched- and ignited-state variances to be equal at $\overline{St} = \overline{St}_i$ is an upper bound; the multiple steady states and the step change in variance with St are thus limited to very small ϕ.

Approximate analytical expressions for the velocity variance in the ignited state can be obtained if we simplify (4.27) by neglecting the last term on the left-hand side of that equation. This yields $T = 0$ for the quenched state and

$$\frac{T^{1/2}}{\gamma a} = \frac{5\pi^{1/2}}{288}\frac{\overline{St}}{\phi\chi}\left[\xi + (\xi^2 + \beta)^{1/2}\right] \tag{4.29}$$

for the ignited state. Here,

$$\xi = (1 + \tfrac{8}{5}\phi\chi)^2 + \frac{768}{25\pi}\phi^2\chi^2 - \frac{12}{\overline{St}^2}, \tag{4.30}$$

$$\beta = 144\left[\frac{256}{25\pi}\frac{\chi^2\phi^2}{\overline{St}^2} - \frac{1}{\overline{St}^4}\right]. \tag{4.31}$$

The difference between the approximate and exact solutions of (4.27) diminishes with increasing St and both agree with the asymptotic expression (3.15) for $St \gg 1$.

For the sake of comparison with the results of numerical simulations in §5, we also present expressions for the shear viscosity and normal stress differences. The components of the particle-phase stress are evaluated by combining (4.15) with (4.19), (4.22), and (4.25)–(4.28). Thus, the particle-phase shear viscosity is given by

$$\sigma_{12} = \gamma\mu_s = -\rho_p\phi T\left[a_{12}(1 + \tfrac{8}{5}\phi\chi) - \frac{16}{5\pi^{1/2}}\phi\chi\gamma T^{-1/2}\right]. \tag{4.32}$$

Note that ω and μ_s depend on $T^{1/2}$ in a nonlinear manner, which is critical for explaining the multiple steady states described earlier. The particle-phase rheology also displays normal stress differences with

$$\frac{P_{11} - P_{22}}{P} = \frac{P_{11} - P_{33}}{P} = \frac{3}{1 + \omega\overline{St}}\,\frac{1 + \frac{8}{5}\phi\chi}{1 + 4\phi\chi}, \tag{4.33}$$

where we have defined the particle-phase pressure tensor P_{ij} and pressure P by $P_{ij} = -\sigma_{ij}$ and $P = (1/3)P_{kk}$. Note that our approximate theory predicts $P_{22} = P_{33}$. The more rigorous theory of Tsao & Koch (1994) including a term of $O(a_{ij}^2)$ shows that in the ignited state at large St and small ϕ the leading-order estimates of the normal stress differences are given by

$$\frac{P_{11} - P_{22}}{P} = \frac{18}{St^2}, \quad \frac{P_{11} - P_{33}}{P} = \frac{117}{7St^2} = \frac{16.71\ldots}{St^2}. \tag{4.34}$$

Thus the actual difference between P_{22} and P_{33} is expected to be small in magnitude compared to the difference between P_{11} and P_{22} or P_{33}. It may be noted that in the limit of large St, $\omega \to \overline{St}/6$, and therefore (4.33) in the limit $\phi \to 0$ agrees with the first equation in (4.34). In other words, the difference between our theory and the dilute theory for the ignited state is relatively small at large St. On the other hand, the quenched-state theory of Tsao & Koch which included the term of $O(\gamma^3)$ in (4.21)

predicts

$$\frac{P_{11}-P_{22}}{P}=\frac{27\pi St+48St^2}{72+9\pi St+16St^2},\qquad \frac{P_{11}-P_{33}}{P}=\frac{72+27\pi St+48St^2}{72+9\pi St+16St^2}, \tag{4.35}$$

and therefore we expect our theory to deviate from the actual results whenever T is smaller than $\gamma^2 a^2$.

5. Dynamic simulations for finite St and $e = 1$

The method for computing hydrodynamic interactions among particles is described in detail in Mo & Sangani (1994) and Sangani & Mo (1994). The velocity of the gas was expressed in terms of flows due to force, torque, and stresslet singularities situated at the centre of the particles plus the flow induced by the lubrication singularities which were determined from the translational and rotational velocities of the particles. This resulted in a total of $17N$ unknowns to be determined. The no-slip boundary condition generated $11N$ equations among these unknowns and the other $6N$ conditions were generated by using finite difference approximations of the equations (2.3) for the linear and angular accelerations of the particles. More specifically, we used

$$\frac{2m}{h}[\boldsymbol{U}(t)-\boldsymbol{U}(t-h/2)]=\boldsymbol{F}(\boldsymbol{x}(t),\boldsymbol{U}(t),\boldsymbol{\Omega}(t)) \tag{5.1}$$

plus a similar equation for the angular momentum balance for each particle. Here, h is the time step, $\boldsymbol{x}$ is the position of the particle, and $\boldsymbol{U}(t-h/2)$ is assumed to be known from the previous time-step calculation. Once the $17N$ resulting equations were solved simultaneously, $\boldsymbol{U}(t+h/2)$ and the position of the particle at $t+h$ were estimated from

$$\boldsymbol{U}(t+h/2)=2\boldsymbol{U}(t)-\boldsymbol{U}(t-h/2), \tag{5.2}$$

$$\boldsymbol{x}(t+h)=\boldsymbol{x}+h\boldsymbol{U}(t+h/2). \tag{5.3}$$

The calculation for the position update using (5.3) was done by a standard hard-sphere molecular dynamics code which takes into account the possible collisions between the particles during the time step h. The velocity $\boldsymbol{U}(t+h/2)$ was updated according to the collision rule if a collision occurred during the move. The time step h was chosen such that on average a particle underwent collisions roughly once in 30 time steps. For smaller St and ϕ, for which the collisions occur less frequently, the calculations were repeated with smaller time steps to check for the accuracy of the trajectory calculations. A typical dynamic simulation was carried out for about 6000 time steps. Various average quantities which included the particle velocity variance, the kinetic and collisional contributions to various stress components, and microstructure parameters such as the radial distribution function, were computed after discarding the results for the first several hundred to several thousand time steps for which the steady state was not yet attained. Finally, all simulations were carried out with 6–8 initial configurations with $N = 54$.

Figure 8 shows $T^{1/2}$ (non-dimensionalized by γa) as a function of St/R_{diss} for $\phi = 0.01$ and $e = 1$. For these simulations, we used $\epsilon_m = 0.01$ which corresponds to $R_{diss} = 1.3$. The solid line shows the prediction of the approximate theory of §4 (cf. (4.27)) while the dashed line corresponds to the asymptotic theory of §3 (cf. (3.15)) for large St. The simulation results indicated by circles are seen to be in excellent agreement with the approximate theory. This theory also predicts an abrupt change

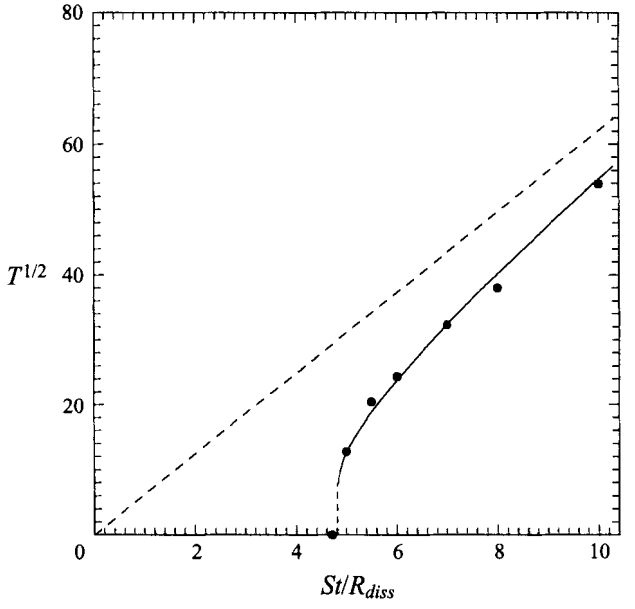

FIGURE 8. $T^{1/2}$ (non-dimensionalized by γa) as a function of St/R_{diss} for $\phi = 0.01$ and $e = 1$. The solid line is the prediction of the approximate theory for the ignited state which predicts the extinction of the ignited state at $St/R_{diss} = 4.8$, the dashed line is the asymptotic theory for large St and circles are the simulation results.

in the variance at St/R_{diss} of ≈ 4.8. Our simulation corresponding to $\overline{St} = 4.7$ indeed resulted in the quenched state. According to the theory of Tsao & Koch (1995), the quenched state T is given by

$$\frac{T}{\gamma^2 a^2} = \frac{64}{945\pi}\overline{St}^3\phi\left[1 + \frac{9\pi}{16}\overline{St}^{-1} + \tfrac{9}{2}\overline{St}^{-2}\right]. \tag{5.4}$$

This expression predicts $T/(\gamma^2 a^2)$ equal to 0.035 for $\phi = 0.01$ and $\overline{St} = 4.7$ whereas our numerical simulations gave an average value of 0.002. As noted by Tsao & Koch, the quenched-state variance is sensitive to the system size with particles in small systems without hydrodynamic interactions eventually taking up positions which reduce the collisions, yielding thereby vanishingly small values of T. The small variance observed in our simulations suggests that the hydrodynamic interactions do not significantly alter this behaviour of the quenched state.

Figure 9(*a*) shows a comparison between the approximate theory and simulations for the particle-phase viscosity μ_s (normalized by $\rho_p \gamma a^2$). As mentioned earlier, throughout this study we have neglected the hydrodynamic contribution to the stress tensor. Thus, μ_s was determined by adding only the kinetic and collisional contributions of the particle-phase stress σ_{12}. As explained earlier, this is reasonable for gas–solid suspensions with relatively large St. The predictions of the approximate theory of §4 shown by the solid line are in excellent agreement with the simulation results. It may be noted that the particle-phase rheology displays a shear-thickening behaviour with the shear viscosity increasing as γ^2 at large St for a given gas–solid system with $e = 1$. (Note that $T^{1/2}$ is proportional to γSt and St is proportional to γ.) Figure 9*b* shows the comparison for the normal stress differences $(P_{11} - P_{22})/P$ and $(P_{11} - P_{33})/P$ as functions of St/R_{diss}. Our approximate theory predicts that the two normal stress differences are equal. The solid line represents these stress differences

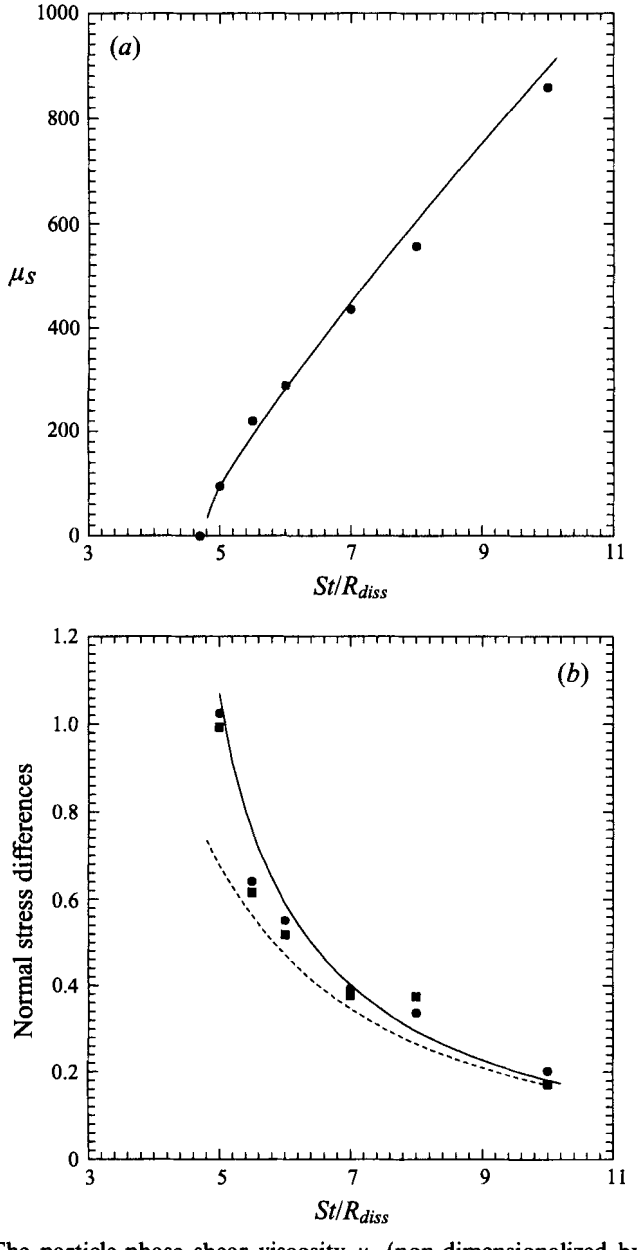

FIGURE 9. (*a*) The particle-phase shear viscosity μ_s (non-dimensionalized by $\rho_p \gamma a^2$) as a function of St/R_{diss} for $\phi = 0.01$ and $e = 1$. The solid line is the prediction of the approximate theory and the circles are the simulation results. (*b*) The normal stress differences, $(P_{11} - P_{22})/P$ (squares) and $(P_{11} - P_{33})/P$ (circles), as functions of St/R_{diss}. The solid line is the approximate theory prediction obtained by solving directly (4.27) while the dashed line is the prediction based on an analytical expression obtained by discarding the last term on left-hand side of (4.27).

obtained by solving the cubic equation (4.27) while the dashed line represents an approximation in which the last term on the left-hand side of (4.27) is neglected so that a closed-form analytical expression for the normal stress differences similar to (4.29) can be obtained. The two methods led to nearly indistinguishable results for T and μ_s shown in figures 8 and 9(*a*), but do result in different predictions for the

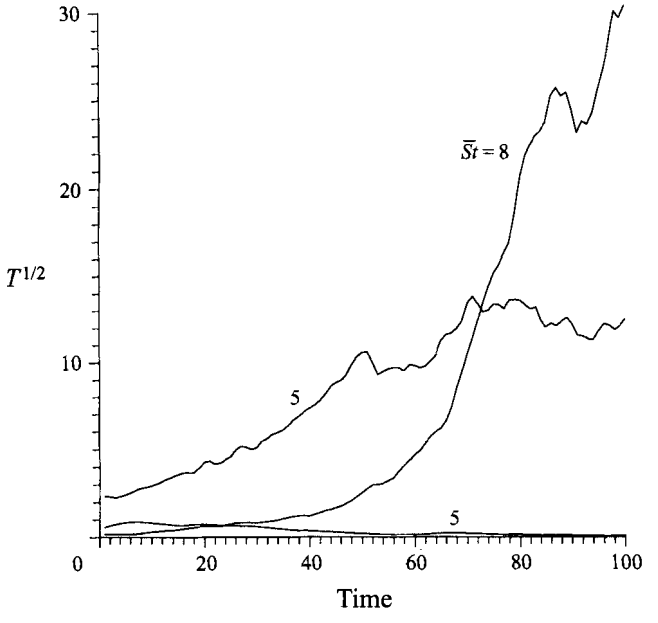

FIGURE 10. $T^{1/2}$ as a function of time for two different values of $\overline{St} = St/R_{diss}$. For $\overline{St} = 5$, we see that the final state depends on the initial T. $\phi = 0.01$ in these simulations.

normal stress differences. The simulation results for the two stress differences are seen to be in good agreement with the approximate theory derived from solving (4.27) exactly. It may be noted that the normal stress differences shown in figure 9*b* are plotted only for $\overline{St} \geqslant 4.8$ for which the final steady state is ignited and therefore the expressions for the quenched state (cf. (4.35)) are not relevant.

The above results were obtained by choosing the initial particle velocity distribution close to that predicted by the theory for the ignited state. For $\phi = 0.01$, there is a narrow range of values of St for which multiple steady states can occur, and, in this range, the final state depends on the initial conditions. This is shown in figure 10 where we plot $T^{1/2}/\gamma a$ as a function of time and initial variance for two different values of St/R_{diss}. For these simulations, we found that at $\overline{St} = 5$ the final state is always a quenched state whenever the initial variance is zero or has a very small value. However, if the initial variance is not small, the final state is the ignited state. On the other hand, the final state for $\overline{St} = 8$ is ignited regardless of the initial variance. For $\overline{St} = 6$ and 7 we found that the final steady state depended on the initial configuration of the particles. For example, of seven configurations with initial zero variance, one led to an ignited state and six to quenched state at $\overline{St} = 6$ while four led to ignited and three to quenched for $\overline{St} = 7$. These simulations were done with a rather small system of 54 particles, and thus the precise value of $\overline{St}_q$ beyond which only the ignited-state solution exists could not be determined accurately. From the above discussion, however, one might expect $\overline{St}_q$ to be between 5 and 8. The direct-simulation Monte Carlo (DSMC) calculations for particles without hydrodynamic interactions conducted by Tsao & Koch (1995) exhibited multiple steady states at $\phi = 0.01$ for a narrow range of Stokes numbers between about 5 and 6. The wider range of Stokes numbers for which multiple steady states are observed in the present dynamic simulations for hydrodynamically interacting particles must result from either the finite size of the system (which has a more serious effect in dynamic than

in DSMC simulations) or from the hydrodynamic interactions attenuating the source of fluctuating energy due to shear-driven collisions.

We now consider non-dilute suspensions. For these dense suspensions only a single steady state is expected. The results for $\phi = 0.1$ are shown in figure 11. The dynamic simulations used $\epsilon_m = 0.01$ which corresponds to $R_{diss} = 2.5$. Once again the results of the approximate theory and the asymptotic theory for large $\overline{St}$ are shown by the solid and dashed lines, respectively. Also shown in the figure is the prediction of the approximate theory with the last term on the left-hand side of (4.27) neglected for which the analytical expressions for T (cf. (4.29)) and the particle-phase stress are easy to obtain. This approximation is indistinguishable from that indicated by the solid line except for small $\overline{St}$ where it is indicated by the dotted line. Finally, the numerical simulation results obtained by incorporating full hydrodynamic interactions indicated by circles are also compared to the simple simulations in which the detailed hydrodynamic interactions are ignored and the particle trajectories are evaluated based on a mean drag law (i.e. $F_i = -6\pi\mu a R_{diss}(U_i - \gamma_{ij}x_j)$). It is interesting that these simple simulations, in which the hydrodynamic interactions are incorporated only by enhancing the drag by a factor obtained from the analysis of the rate of energy dissipation in a hard-sphere system described in §3.1, give remarkably accurate estimates of various average quantities even when $\overline{St}$ is as small as 3. We see that the variance predicted from the approximate theory is slightly below that obtained from numerical simulations at small $\overline{St}$. This slight difference could have resulted from neglecting the higher-order terms in the expression for $S(C_iC_j)$ used in our theory. It is interesting to note that the difference between the asymptotic theory and the approximate theory is much smaller for $\phi = 0.1$ than for $\phi = 0.01$. Figure 11(*c*) shows the kinetic and collisional contributions to the particle-phase shear viscosity, or equivalently σ_{12}. The solid lines indicate the predictions of the approximate theory. We see that the theory accurately predicts not only the overall properties such as T and μ_s but also the relative importance of the kinetic and collisional contributions to the stress. Finally, the normal stress differences are plotted in figure 11(*d*). Here, the filled symbols indicate results obtained by simulations including the detailed hydrodynamic interactions while the open symbols indicate results obtained from simple simulations using the mean drag law. The solid line represents the prediction of the approximate theory developed in the present study which gives equal normal stress differences, i.e. $P_{22} = P_{33}$, while the dashed lines represent the theory of Tsao & Koch for the quenched state in which T is small compared to γ^2a^2. We see that the approximate theory developed here begins to fail only for St/R_{diss} less than about 3. The simulation results for $St/R_{diss} = 1$ for which $T/(\gamma^2a^2)$ is small compared to 1 are seen to be in qualitative agreement with the small-ϕ small-T theory of Tsao & Koch (cf. (4.35)).

The results for $\phi = 0.25$ and $e = 1$ are shown in figure 12. These results were obtained with $\epsilon_m = 0.01$ which corresponds to $R_{diss} = 5.0$. We see that the difference between the asymptotic theory and the approximate theory is further reduced and that the results of simulations are once again in very good agreement with those predicted by the theory. Also the results obtained with simulations using the mean drag law are once again seen to be in excellent agreement with those obtained by the simulations which account for the hydrodynamic interactions. Note also that since R_{diss} increases with increasing ϕ, $St = \overline{St}R_{diss}$ also increases for a given value of $\overline{St}$. As a result the particles are expected to travel in a nearly straight line between the successive collisions for dense suspensions, and this should result in a better agreement between the results of simulations which include the effects of hydrodynamic interactions on the dynamic particle motion and those that only incorporate their influence on the

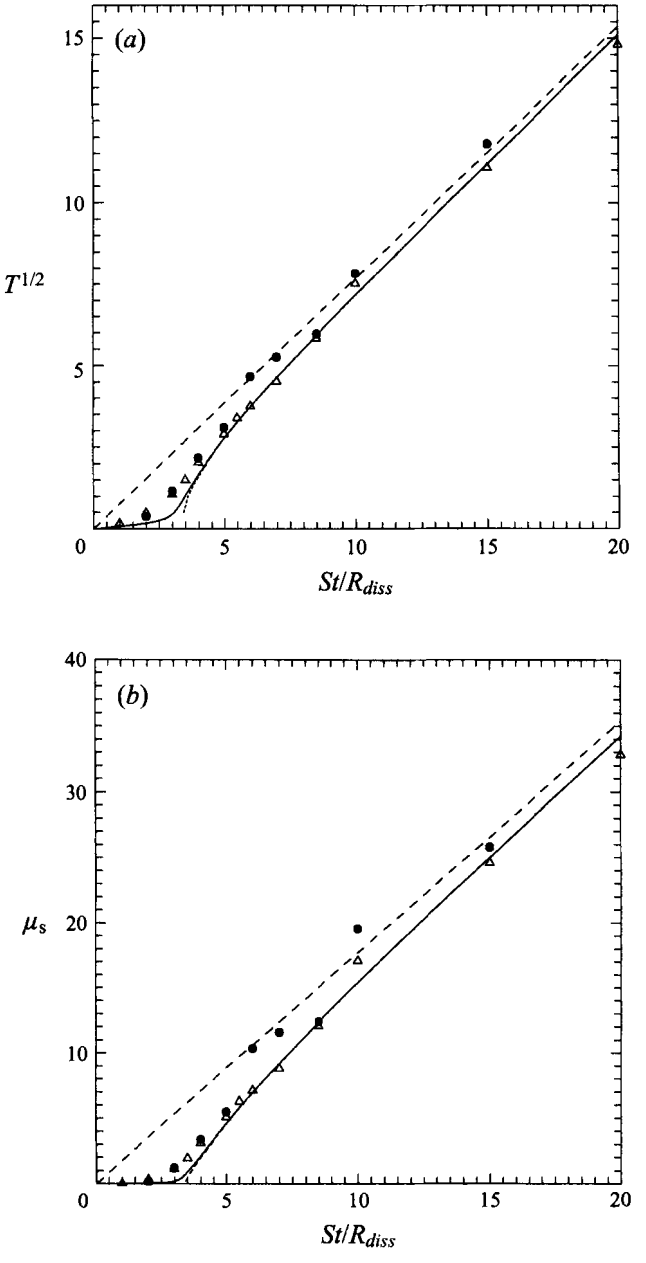

FIGURE 11(*a,b*). For caption see facing page.

rate of energy dissipation in a hard-sphere suspension. It is also important to note that the magnitude of the normal stress differences for $\phi = 0.25$ (cf. figure 12*c*) are small compared to those found for $\phi = 0.1$. Also, in general, the normal stress difference $(P_{11} - P_{22})$ indicated by squares is more closely predicted by the approximate theory than is $P_{11} - P_{33}$ indicated by circles in figures 11(*d*), 12(*c*), and 13(*b*). Finally, the results for $\phi = 0.45$ are shown in figure 13. For these simulations, we used $\epsilon_m = 0.01$ which corresponds to $R_{diss} = 11.2$. The approximate and asymptotic theory predictions for T are nearly equal and thus indistinguishable for this case. The simulation results

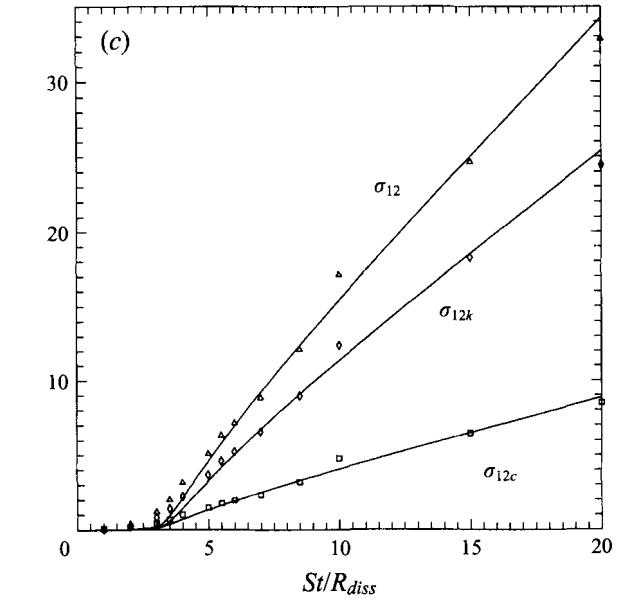

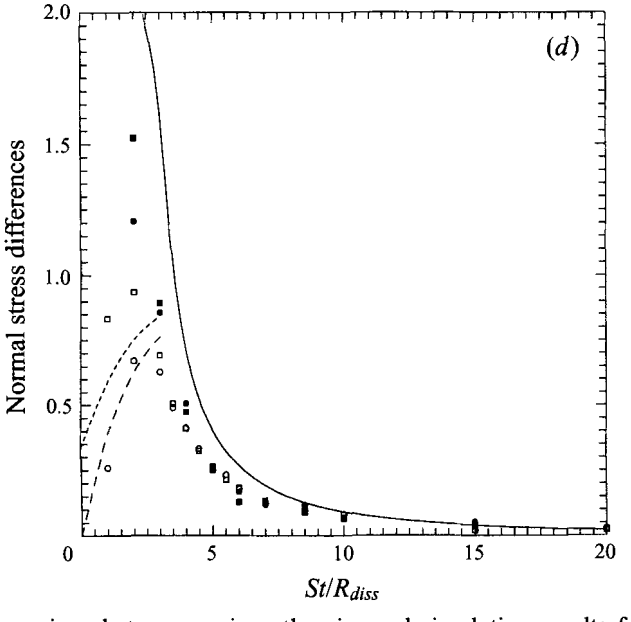

FIGURE 11. Comparison between various theories and simulation results for $\phi = 0.1$ and $e = 1$. The solid line represents the approximate theory predictions, the dashed line represents the large St asymptotic theory and the dotted line represents the simplified approximate theory obtained by neglecting the last term on the left-hand side of (4.27). The filled symbols represent the results from the detailed hydrodynamic interaction simulations while the unfilled symbols represent the results from simulations using the mean drag law. (*a*) $T^{1/2}$ as a function of R_{diss}; (*b*) the particle-phase shear viscosity μ_s as a function of St/R_{diss}; (*c*) the kinetic (*k*) and collisional (*c*) contributions to the particle-phase shear stress σ_{12} (non-dimensionalized by $\rho_p\gamma^2a^2$); (*d*) normal stress differences $(P_{11} - P_{22})/P$ (squares) and $(P_{11} - P_{33})/P$ (circles). In (*d*) the dashed lines correspond to the theory of Tsao & Koch for $T \ll \gamma^2a^2$ (cf. (4.35)).

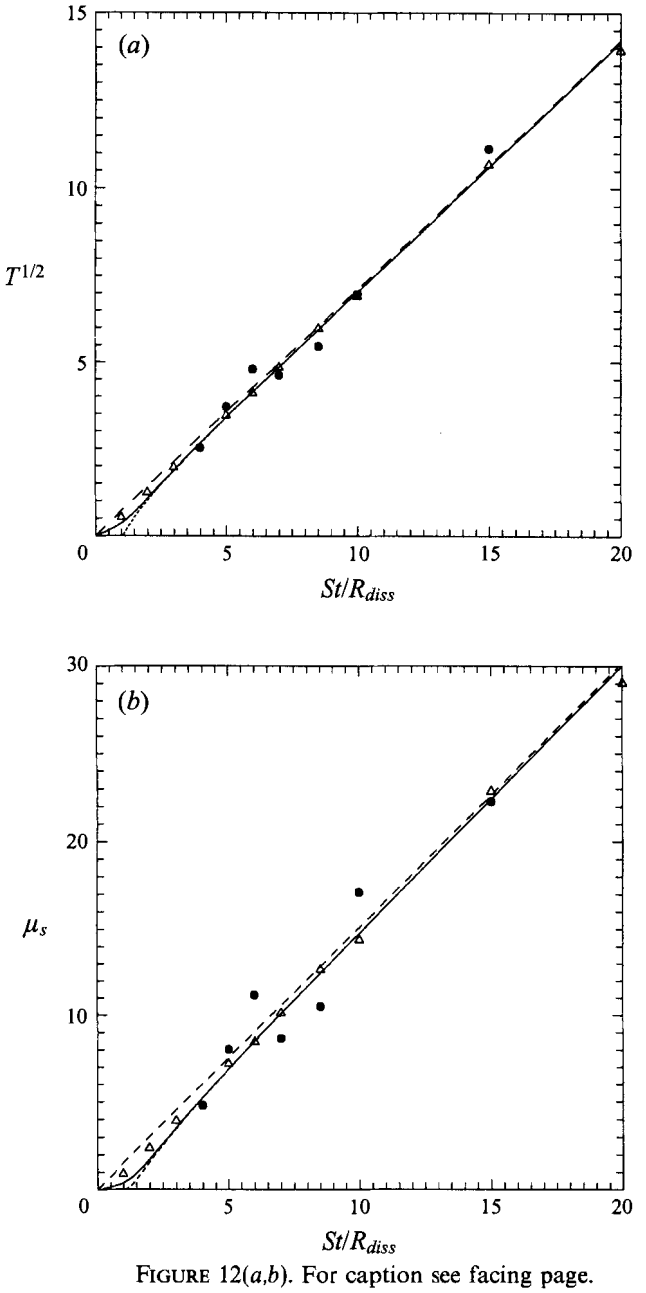

FIGURE 12(*a*,*b*). For caption see facing page.

for T are seen to be slightly higher than the theoretical predictions with a maximum deviation in $T^{1/2}$ of about 20% at $\overline{St} = 5$. We have analysed various microstructure-related quantities, such as radial distribution function, in an attempt to understand the origin of this difference between the predictions of the theory and the results of simulations, but have found no significant difference between the microstructure of the sheared suspensions and the equilibrium hard-sphere systems. The results for normal stress differences are shown in figure 13(*b*). Although the scatter in numerical simulation results is too large to test the theoretical predictions, we see that the

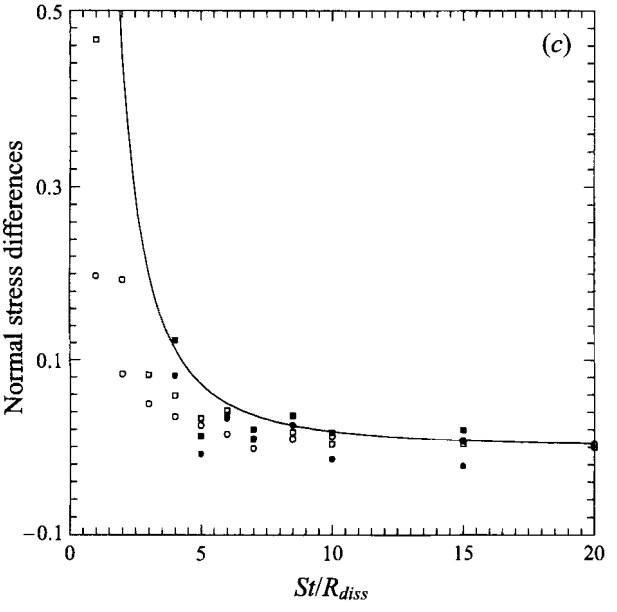

FIGURE 12. Comparison of various theories and simulation results for $\phi = 0.25$ and $e = 1$. Refer to figure 11 caption for the symbol and line conventions.

magnitude of the normal stress difference is generally small for such high ϕ. This trend of decreasing normal stress differences with increasing volume fraction at a fixed value of St/R_{diss} is similar to the observation that the normal stress difference in granular flow decreases with the increase in ϕ at a fixed value of e (Walton & Braun 1986). Note that this trend of decreasing normal stress differences with increasing ϕ is opposite to that for the zero Stokes number suspensions for which the normal stress differences increase with ϕ. In the latter case the stresslet induced by the presence of the particles determines the magnitude of the particle stress.

In addition to comparing the prediction of various average quantities with the predictions of the theory, we can also do a more detailed analysis of the assumptions used in developing the approximate theory. For example, the theory ignored the dissipation resulting from the fluctuations in the angular velocity. For $\phi = 0.25$ and $St/R_{diss} = 10$, our detailed simulations gave the value of $\langle \boldsymbol{F} \cdot \hat{\boldsymbol{U}} \rangle / \langle \boldsymbol{L} \cdot \hat{\boldsymbol{\Omega}} \rangle$, which represents the ratio of energy dissipation by fluctuations in translational and rotational velocities, of about 250. Here, a hat represents the fluctuation from the mean value and $\boldsymbol{L}$ is the torque acting on the particles. The values of the same ratio at $\phi = 0.45$ for St/R_{diss} equal to 5, 7 and 10 were found to be, respectively, 1533, 865, and 771. Also, we found that $\langle U^2 \rangle / \hat{\Omega}^2 a^2 = 1167$ at $\phi = 0.45$ and $St/R_{diss} = 7$.

6. Theory and simulations for finite inelasticity and finite St

We now consider the more general case of simple shear flows of gas–solid suspensions with finite viscous and inelasticity effects. We will express the root-mean square of the fluctuations in terms of ω_η defined by

$$\omega_\eta = \frac{24}{5\pi^{1/2}} \phi \chi \eta (2 - \eta) \frac{T^{1/2}}{\gamma a}. \tag{6.1}$$

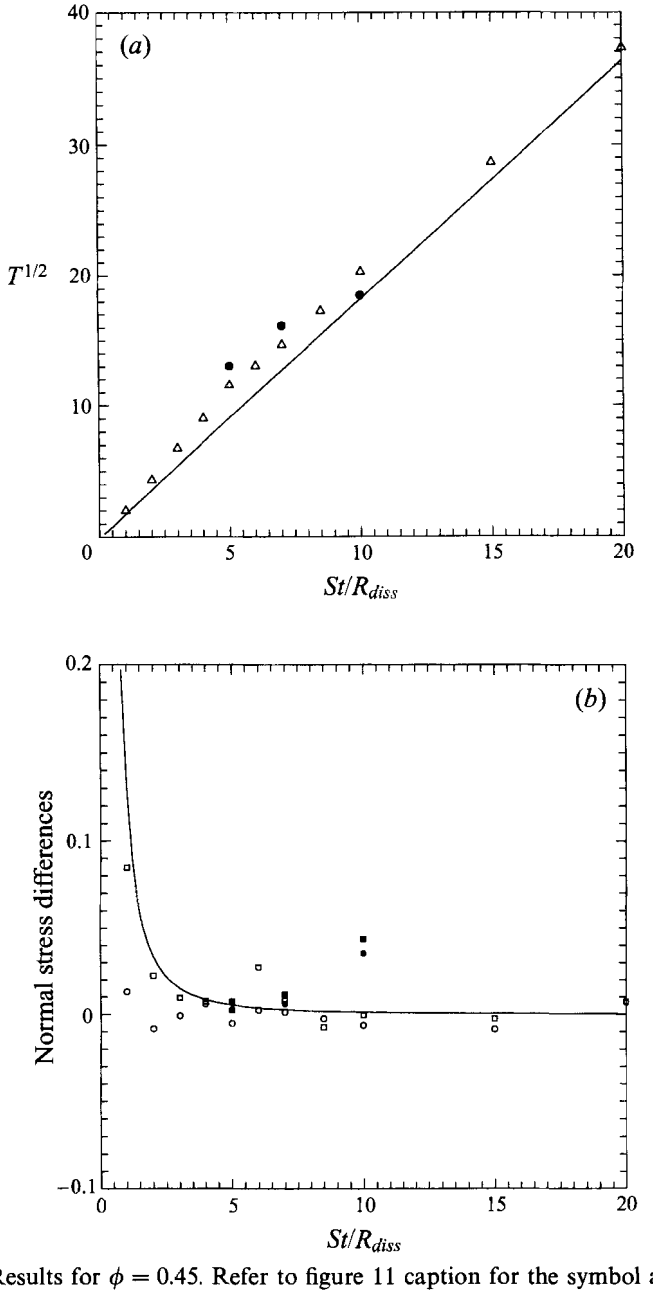

FIGURE 13. Results for $\phi = 0.45$. Refer to figure 11 caption for the symbol and line conventions.

Substituting for γ_{ij} from (4.24) into (4.23) and solving the resulting equation together with the condition $a_{ii} = 0$ yields

$$a_{22} = a_{33} = -\tfrac{1}{2}a_{11} = -\frac{5\omega_\eta(1-\eta) + 3(2-\eta)\overline{St}^{-1}}{3(2-\eta)(\omega_\eta + \overline{St}^{-1})}, \tag{6.2}$$

$$a_{12} = \frac{1}{1+\frac{8}{5}\phi\chi\eta}\left[3a_{22}(\omega_\eta + \overline{St}^{-1}) + \phi^2\frac{\alpha}{\omega_\eta}\right], \qquad \alpha = \frac{384}{25\pi}\chi^2\eta^2(2-\eta). \tag{6.3}$$

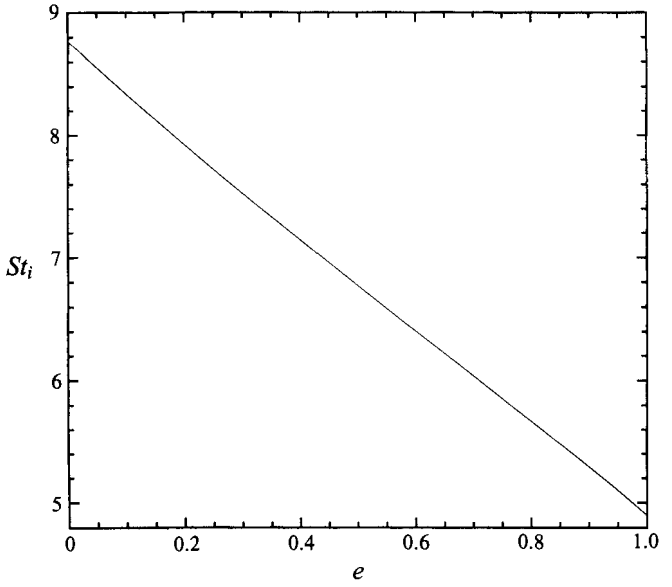

FIGURE 14. The critical value of St below which the ignited state ceases to exist as a function of the coefficient of restitution e for dilute ($\phi \to 0$) suspensions.

The reduced root-mean-square of the fluctuations now satisfies the quartic equation

$$\sum_{n=0}^{4} d_n \omega_\eta^n = 0 \tag{6.4}$$

with

$$d_4 = 15(1-\eta), \qquad d_3 = (48-39\eta)\overline{St}^{-1}, \tag{6.5}$$

$$d_2 = 3[(17-11\eta)\overline{St}^{-2} - \phi^2\alpha] - \tfrac{1}{2}\left(1+\tfrac{8}{5}\phi\chi\right)\left\{2\eta+1-\tfrac{8}{5}\phi\chi(9\eta^3-24\eta^2+7\eta+5)\right\}, \tag{6.6}$$

$$d_1 = 3(2-\eta)\overline{St}^{-1}\left[3\overline{St}^{-2} - 2\alpha\phi^2 + \tfrac{4}{5}\phi\chi\left(1+\tfrac{8}{5}\phi\chi\right)(1-\eta)(3\eta+1)\right], \tag{6.7}$$

$$d_0 = -3\alpha\phi^2\overline{St}^{-2}(2-\eta). \tag{6.8}$$

Equations (6.2)–(6.4) reduce to (4.25)–(4.27) for the special case of elastic particles, i.e. $\eta = (1+e)/2 = 1$. For small ϕ, d_0 can be set to zero and the resulting quartic equation has four real roots for $St > St_i(e)$, one negative, one corresponding to a quenched state $\omega_\eta = 0$, and two positive. St_i is determined from the condition that the two real positive roots are equal at $St = St_i$. The results are shown in figure 14. The variation of St_i with e is nearly linear

$$St_i \approx 8.7 - 3.8e. \tag{6.9}$$

The approximate theory for finite St and $1-e$ can be tested once again with the results obtained from numerical simulations. As the results of the previous section show, the most critical test of the theory can be made at smaller values of ϕ where the deviation between the approximate theory and the asymptotic theory based on Newtonian rheology is the greatest. Therefore, we carried out simulations only for $\phi = 0.01$. The results are shown in figure 15 where we see that the simulations are in very good agreement with the theoretical predictions. These simulations were carried

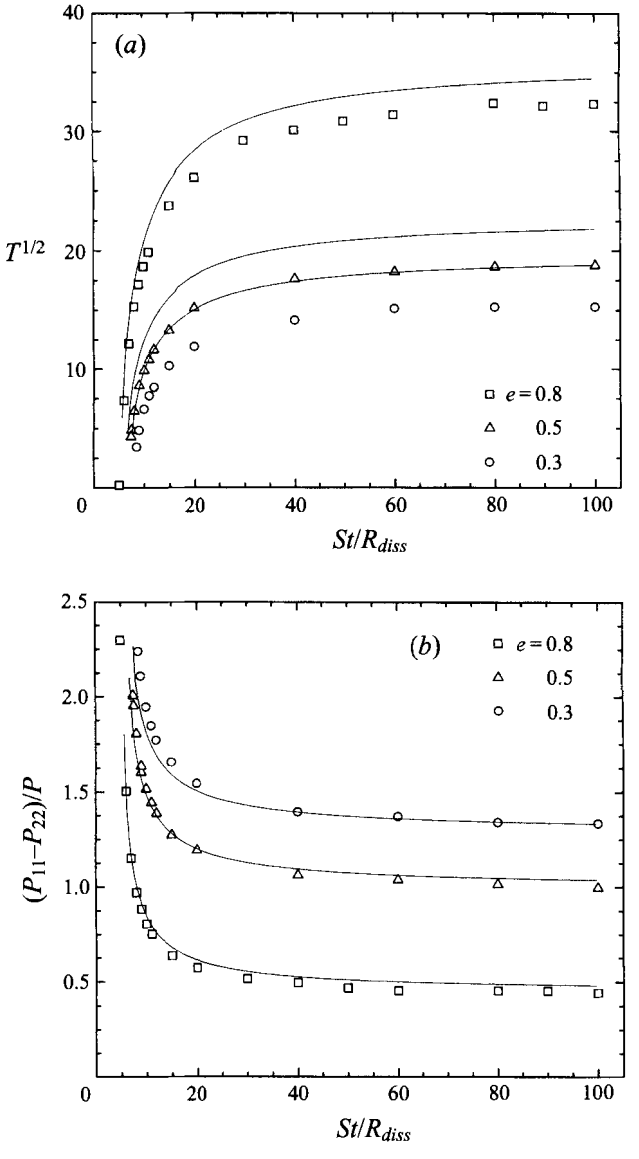

FIGURE 15(*a*,*b*). For caption see facing page.

out by neglecting hydrodynamic interactions as our earlier calculations show that the detailed hydrodynamic interactions do not affect the results. At any rate, we have also carried out a few simulations with detailed hydrodynamic interactions and found essentially the same results.

7. Concluding remarks

We have extended the theory of rapidly sheared granular flows in which the effects of the inelastic particle collisions dominate to flows with significant viscous effects. The approximation derived using Grad's moment method to solve for the particle velocity distribution function is shown to give surprisingly accurate results even when the particle-phase temperature T is not much larger than $\gamma^2 a^2$. The good agreement

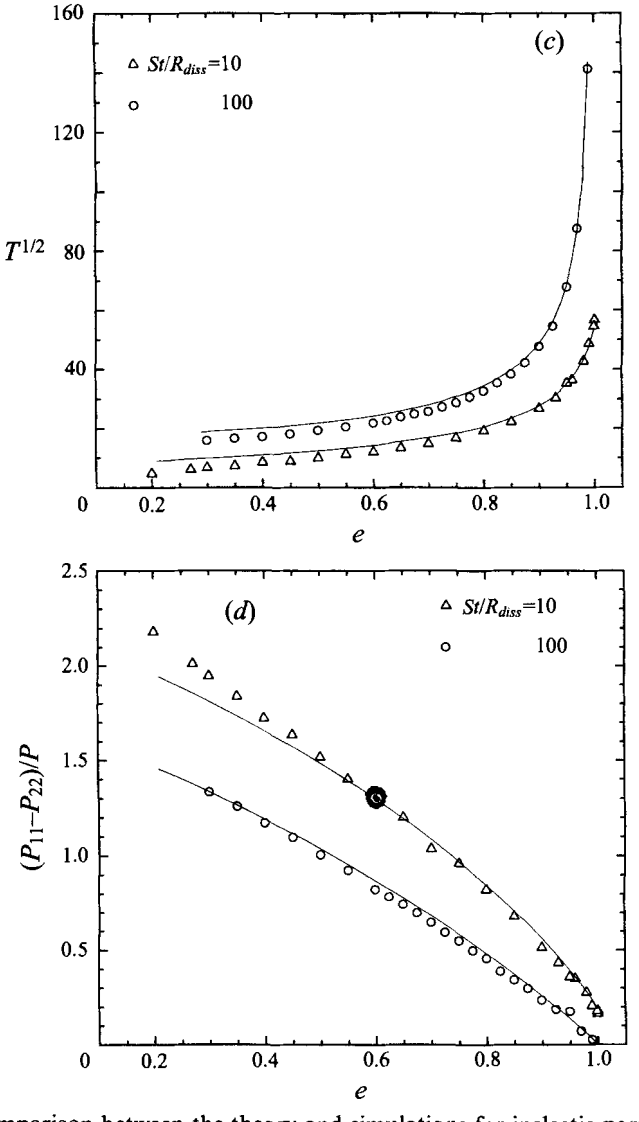

FIGURE 15. Comparison between the theory and simulations for inelastic particles with finite Stokes numbers at $\phi = 0.01$. (*a*) $T^{1/2}$ versus St/R_{diss}; (*b*) $(P_{11} - P_{22})/P$ versus St/R_{diss}; (*c*) $T^{1/2}$ versus e; (*d*) $(P_{11} - P_{22})/P$ versus e.

between our theory and numerical simulations indicates that hydrodynamic interactions can be incorporated in the theory of rapidly sheared particulate suspensions in a fully analytic manner through R_{diss} given by (3.17), (3.22), and (3.24).

The simulations were carried out with a rather small system of 54 particles in a periodic box since calculation of the detailed hydrodynamic interactions are computationally very expensive. The studies of granular flows with much large systems by Hopkins & Louge (1991), Walton, Kim & Rosato (1991), and Hopkins, Jenkins & Longe (1991) have shown that homogeneous granular suspensions are unstable in the presence of mean shear, and that large anisotropic clusters form as a consequence. The imposed periodicity can have a significant stabilizing influence, and thus even if such instabilities were to exist in viscous suspensions, it would not have

been possible to observe them in our simulations with small systems. We plan to address the problem of stability of gas–solid suspensions with significant viscous effects through a linear stability analysis of the average equations of motion in our future work.

This work was supported in part by a grant NAG3-1630 from NASA. A.S.S. and G.M. also acknowledge the support by NSF through the grant CTS-9307723. D.L.K. acknowledges the support by the US Environmental Protection Agency through the grant R81-9761-010. All computations were performed on the Cornell National Supercomputer Facility.

REFERENCES

BABIC, M. 1993 On the stability of rapid granular flows. *J. Fluid Mech.* **254**, 127–150.

BARNOCKY, G. & DAVIS, R. H. 1989 The influence of pressure-dependent density and viscosity on the elastohydrodynamic collision and rebound of two spheres. *J. Fluid Mech.* **209**, 501–519.

BRADY, J. F. & BOSSIS, G. 1988 Stokesian dynamics. *Ann. Rev. Fluid Mech.* **20**, 111–157.

BULTHUIS, H., PROSPERETTI, A. & SANGANI, A. S. 1995 'Particle stress' in disperse two-phase potential flow. *J. Fluid Mech.* **294**, 1–16.

CAMPBELL, C. S. 1989 The stress tensor for simple shear flows of a granular material. *J. Fluid Mech.* **203**, 449–473.

CARNAHAN, N. F. & STARLING, K. E. 1969 Equation of state for non-attracting rigid spheres. *J. Chem. Phys.* **51**, 635–636.

CHAPMAN, S. & COWLING, T. G. 1970 *The Mathematical Theory of Non-Uniform Gases*, 3rd Edn. Cambridge University Press.

GADALA-MARIA, F. A. & ACRIVOS, A. 1980 Shear-induced structure in a concentrated suspension of solid spheres. *J. Rheol.* **24**, 799–814.

GRAD, H. 1949 On the kinetic theory of rarified gas. *Commun. Pure Appl. Maths* **2**, 331–407.

HINCH, E. J. 1977 An averaged-equation approach to particle interactions in a fluid suspension. *J. Fluid Mech.* **83**, 695–720.

HOPKINS, M. A., JENKINS, J. T. & LOUGE, M. Y. 1991 On the structure of 3D shear flows. In *Micromechanics of Granular Materials* (ed. H. H. Shen & M. Satake). Elsevier.

HOPKINS, M. A. & LOUGE, M. Y. 1991 Inelastic microstructure in rapid granular flows of smooth disks. *Phys. Fluids* A **3**, 47–57.

HOWELLS, I. D. 1974 Drag due to the motion of a Newtonian fluid through a sparse random array of small fixed objects. *J. Fluid Mech.* **64**, 449–475.

JENKINS, J. T. & RICHMAN, M. W. 1985 Grad's 13-moment system for a dense gas of inelastic spheres. *Arch. Rat. Mech. Anal.* **87**, 355–377.

JENKINS, J. T. & SAVAGE, S. B. 1983 A theory for the rapid flow of identical, smooth, nearly elastic particles. *J. Fluid Mech.* **130**, 187–202.

KIM, S. & KARRILA, S. P. 1991 *Microhydrodynamics: Principles and Selected Applications.* Butterworth-Heinemann.

KIM, S. & RUSSELL, W. B. 1985 Modelling of porous media by renormalization of the Stokes equations. *J. Fluid Mech.* **154**, 269–286.

KOCH, D. L. 1990 Kinetic theory for a monodisperse gas-solid suspension. *Phys. Fluids* A **2**, 1711–1723.

KREMER, G. M. & ROSA, E. 1988 On Enskog's dense gas theory. I. The method of moments for monatomic gases. *J. Chem. Phys.* **89**, 3240–3247.

LADD, A. J. C. 1990 Hydrodynamic transport coefficients of random dispersions of hard spheres. *J. Chem. Phys.* **95**, 3484–3494.

LUN, C. K. K., SAVAGE, S. B., JEFFREY, D. J. & CHEPURNEY, N. 1984 Kinetic theories for granular flow: inelastic particles in a Couette flow and slightly inelastic particles in a general flow field. *J. Fluid Mech.* **140**, 223–256.

MA, D. & AHMADI, G. 1988 A kinetic model for rapid granular flows of nearly elastic particles including interstitial fluid effects. *Powder Technol.* **56**, 191–207.

Mo, G. & Sangani, A. S. 1994 A method for computing Stokes flow interactions among spherical objects and its application to suspensions of drops and porous particles. *Phys. Fluids* **6**, 1637–1652.

Nott, P. R. & Brady, J. F. 1994 Pressure-driven flow of suspensions: simulation and theory. *J. Fluid Mech.* **275**, 157–199.

Sangani, A. S. & Didwania, A. K. 1993 Dispersed-phase stress tensor in flows of bubbly liquids at large Reynolds numbers. *J. Fluid Mech.* **248**, 27–54.

Sangani, A. S. & Mo, G. 1994 Inclusion of lubrication forces in dynamic simulations. *Phys. Fluids* **6**, 1653–1662.

Smart, J. R. & Leighton, D. T. 1989 Measurement of the hydrodynamic surface roughness of noncolloidal spheres. *Phys. Fluids* A **1**, 52–60.

Sundararajakumar, R. R. & Koch, D. L. 1996 Non-continuum lubrication flows between particles colliding in a gas. *J. Fluid Mech.* **313**, 283–308.

Tsao, H.-K. & Koch, D. L. 1995 Rapidly sheared, dilute gas- solid suspensions. *J. Fluid Mech.* **296**, 211–245.

Walton, O. R. & Braun, R. L. 1986 Stress calculations for assemblies of inelastic spheres in uniform shear. *Acta Mech.* **63**, 73–86.

Walton, O. R., Kim, H. & Rosato, A. D. 1991 Microstructure and stress differences in shearing flows. *Mechanics Computing in 1990s and Beyond* (ed. H. Adeli & R. L. Sierakowski). *Proc. E.M. Div–ASCE, Columbus, OH*, pp. 1249–1253.

Woodcock, L. V. 1981 Glass transition in the hard-sphere model and Kauzmann's paradox. *Ann. NY Acad. Sci.* **371**, 274–298.

Zhang, D. Z. & Prosperetti A. 1994 Averaged equations for inviscid disperse two-phase flow. *J. Fluid Mech.* **267**, 185–219.